Report 93226
August 6, 1986
NAS 5-29276

FINAL REPORT

ISTP SBIR PHASE I

FULL-SKY SCANNER

A FEASIBILITY STUDY

Prepared for:

NASA
Goddard Space Flight Center
Greenbelt, MD 20771
Under Contract No.: NAS5-29276

Prepared by:

ITHACO, Inc.
735 W. Clinton Street
P.O. Box 6437
Ithaca, NY 14851-6437

SBIR RIGHTS NOTICE (APRIL 1986)

This SBIR data is furnished with SBIR rights under NASA Contract No. NAS5-29276. For a period of two years after acceptance of all items to be delivered under this contract, the Government agrees to use this data for Government purposes only, and it shall not be disclosed outside the Government (including disclosure for procurement purposes) during such period without permission of the Contractor, except that, subject to the foregoing use and disclosure prohibitions, such data may be disclosed for use by support contractors. After the aforesaid two-year period, the Government has a royalty-free license to use, and to authorize others to use on its behalf, this data for Government purposes, but is relieved of all disclosure prohibitions and assumes no liability for unauthorized use of this data by third parties. This Notice shall be affixed to any reproductions of this data, in whole or in part.

PROJECT SUMMARY

Purpose

To develop a Full-Sky Sensor (FSS) to detect the Earth, Sun and Moon from a spinning spacecraft. This sensor, with ground processing, must be capable of accurately locating the centroid of these bodies from low orbits to the L1 libration point. Coverage must be 4π steradians with provisions for recognizing or blanking spacecraft appendages.

Concept

The concept adopted has infinitely variable resolution. A high-speed search mode is implemented on the spacecraft. A stepping sensor with 0.2° steps was the original concept but this was discarded early in the program for reasons presented in this report.

Findings and Results

The attitude determination accuracy will be as follows:

Low Earth Orbit (<1,000 km)	<0.2° 3 sigma (Earth) <0.03° 3 sigma (Sun)
L1 Libration Point	<0.1° 3 sigma (Earth) <0.1° 3 sigma (Moon) <0.03° 3 sigma (Sun)

Advantages

1) A single sensor determines attitude parameters from Earth, Sun and Moon; thus eliminating instrument mounting errors.
2) The bias between the actual spacecraft spin axis and the intended spin axis can be determined.
3) Cost is minimized.
4) Ground processing is straight forward.

Hardware Feasibility

The FSS is a modification of an existing flight-proven sensor. Signal levels for the various missions have been determined, and the signal-to-noise levels are satisfactory with the modifications proposed. Mechanical changes are minimal. Modification to the electronics are necessary to accommodate the amplitude range and signal width range of the celestial bodies to be detected.

Potential Applications

1) All ISTP missions, including the Japanese GEOTAIL and the European CLUSTER missions.
2) MSSP (Multi-Spacecraft Satellite Program).
3) Dual-spin spacecraft at any altitude.
4) Spinning spacecraft at any altitude.
5) In low-Earth orbits, this sensor has the potential for determining all orbit parameters.

ACKNOWLEDGEMENTS

1. To the ISTP team at the Goddard Space Flight Center for the wherewithal for this analysis.

2. To Dr. James Wertz and Tom Mullikin for the inputs, analysis and guidance that they have provided.

3. A special tribute to Dr. Leonard Smithline who passed away in November 1985. Dr. Smithline provided much of the early conceptualization for the Full-Sky Scanner, which set the direction of the program.

REFERENCES

[1] ITHACO Report #90942, LUNAR SURFACE TEMPERATURE.

[2] General Software Corp., GSC-TR8401, LANDSAT 4 HORIZON SCANNER PERFORMANCE EVALUATION.

[3] ITHACO Report #92575, Rev. A, CES NOISE ANALYSIS.

TABLE OF CONTENTS

TABLE OF CONTENTS (CONT'D)

1.0 OBJECTIVES

The objective of the research carried out was to establish the feasibility of incorporating proven technology to configure a full-sky (4π steradian) sensor. The sensor would locate the Earth, Sun and Moon for a spinning spacecraft. The sensor must provide sufficient resolution to accurately identify the attitude of the spacecraft at distances as far as the L1 libration point and as close as the shuttle orbit.

2.0 SCOPE

This study was conducted to determine the feasibility of producing a low cost, 4π steradian, three-body sensor as described in Section 1.0. All relevant issues related to the sensor and applications were addressed.

The following topics were covered during the study:

A. Signal Level Analysis
   - Earth at L1
   - Moon at L1

B. Horizon Locator

C. Detector Evaluation

D. Motor Assessment

E. Accuracy Analysis

F. Bias Determination Analysis

G. Operating Modes

H. Command/Telemetry Requirements

I. Ground Processing
   - Algorithm for determining the centroid of an object
   - Correction for the lunar terminator
   - Global geometry to determine attitude

J. Application to the ISTP Missions
   - WIND
   - EQUATOR
   - POLAR

Tasks F, I, J and part of E and G were performed under the direction of Dr. Jim Wertz. His work was internally funded by ITHACO.

3.0 BACKGROUND

ITHACO has been in the horizon sensor business for more than 20 years. Our original approach to this problem was to develop a stepper sensor with the required 0.2° resolution as a modification of our existing Steerable Horizon Crossing Indicator (SHCI). A pair of the present sensors has been flying on the USAF P78-2 spacecraft since 1979. Attached is a copy of IPS 1-4/79, a sales brochure of ITHACO's SHCI.

The SHCI utilizes a stepper motor with 3° step sizes. As the motor is positioned to a particular angle, the spinning spacecraft rotates about its spin axis causing a cone to be scanned though space. The scan would appear as a latitudinal line on a celestial sphere in spacecraft coordinates. When the angle between the spin axis and the Field of View (FOV) is changed, by changing the position of the motor, a new cone would be scanned. Refer to Figure 3.0-1 for the orientation of the sensor on the spacecraft.

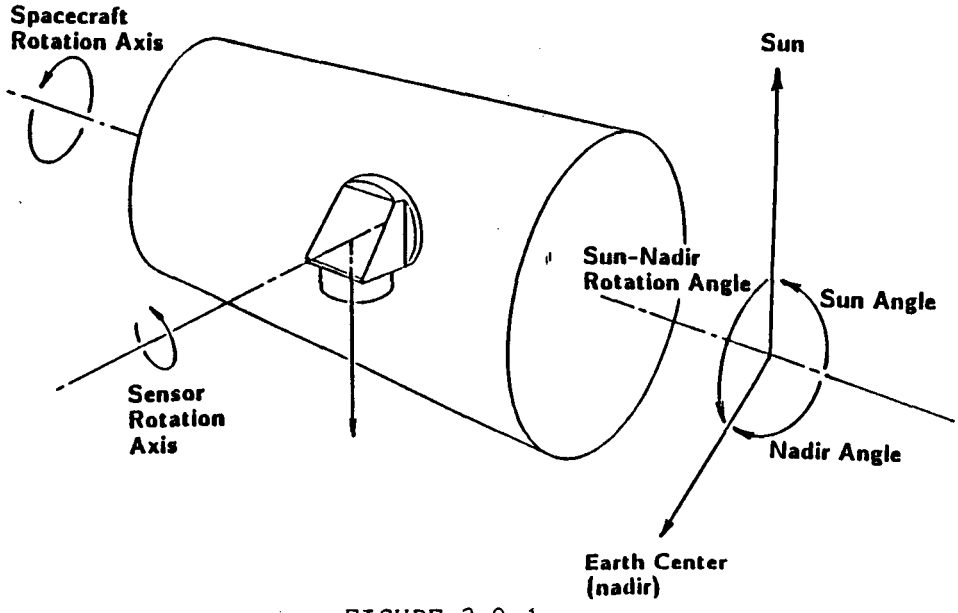

FIGURE 3.0-1
SENSOR MOUNTED ON SPACECRAFT

At lower Earth orbits, the 3° resolution between steps is more than adequate to accurately determine the attitude of a spacecraft. At 250 Earth radii, the Earth is 0.5 degrees; thus, the resolution of the SHCI is not adequate.

Early in the Phase I study, possible solutions to this problem of resolution were pursued. Sophisticated gearing and stepping techniques were investigated, but a superior method was found and pursued. This method involves the use of a Brushless DC motor.

The use of the Brushless DC motor in the Full-Sky Scanner will be explained in detail in Section 4.1. Other options that were investigated are presented in Section 4.10.

4.0 TECHNICAL PRESENTATION

4.1 Basic Concept of the Full-Sky Scanner

The Full-Sky Scanner (FSS) is conceptually similar to ITHACO's Steerable Horizon Crossing Indicator (SHCI). The difference between the two devices allows detection of the Earth and Moon as far away as 250 Earth radii.

The FSS consists of a rotating mirror, an optical barrel, an infrared detector, a Brushless DC motor, a sun sensor and appropriate electronics (refer to Figure 4.1-1). The optical barrel focuses a one-degree field of view (FOV) on the infrared detector. The rotating mirror is attached to the Brushless DC motor, enabling the FOV to scan at a speed controlled by the electronics. The Sun sensor is included for measuring the spacecraft spin rate and to provide a rotational reference.

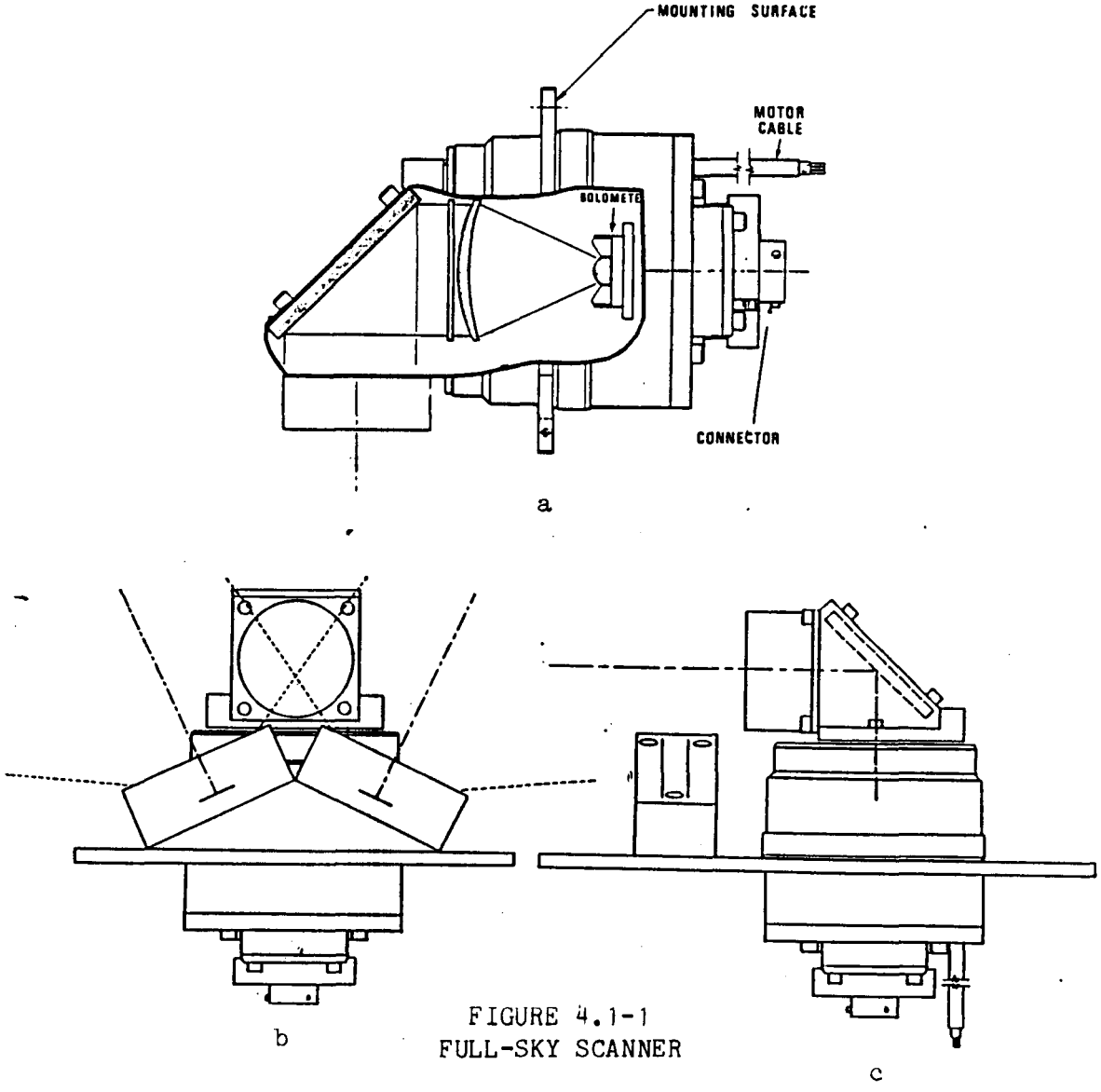

FIGURE 4.1-1
FULL-SKY SCANNER

a) Cutaway Showing Bolometer and Optics.
b) Scanner and Sun Sensor (as seen from side of spacecraft).
c) Scanner and Sun Sensor (looking along spin axis of spacecraft).

The FSS is mounted on the spacecraft orthogonal to the spin axis (refer to Figure 4.1-2). If the spacecraft were not rotating, then the scanner's FOV would sweep out a plane in space. Looking at the scan trace on a celestial sphere, one would see a great circle.

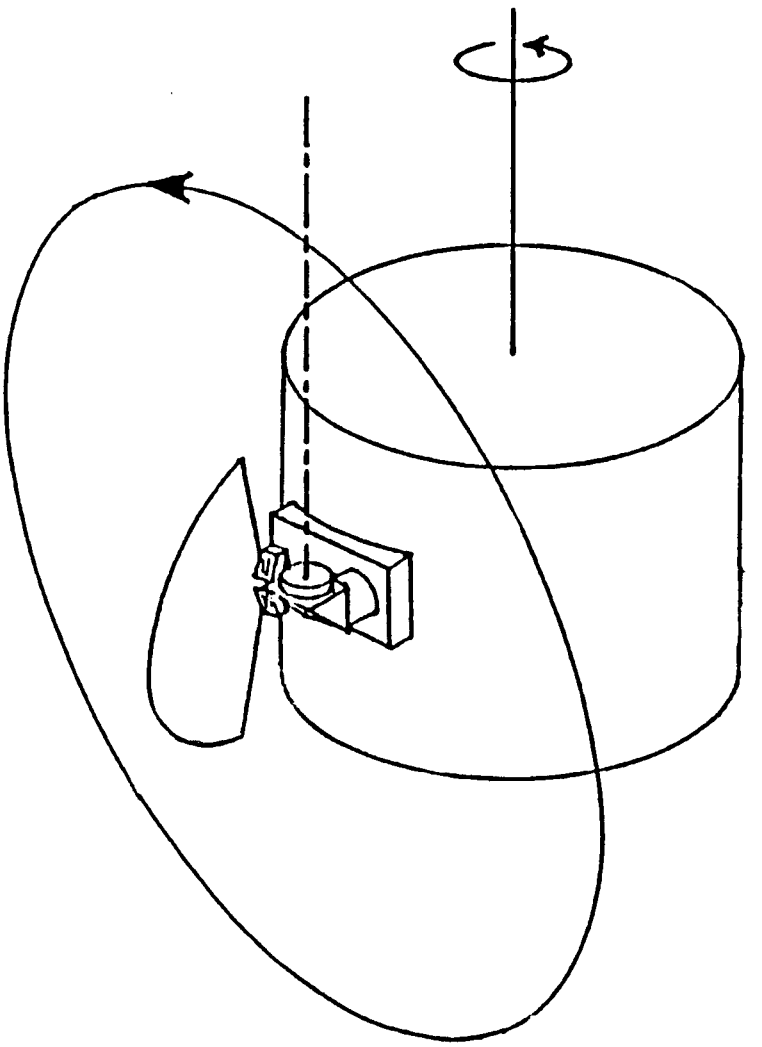

FIGURE 4.1-2
FULL-SKY SCANNER MOUNTING GEOMETRY

Controlling the scan rate such that it equals the spin rate of the spacecraft, a figure "8" scan pattern will be produced on a celestial sphere (refer to Figure 4.1-3).

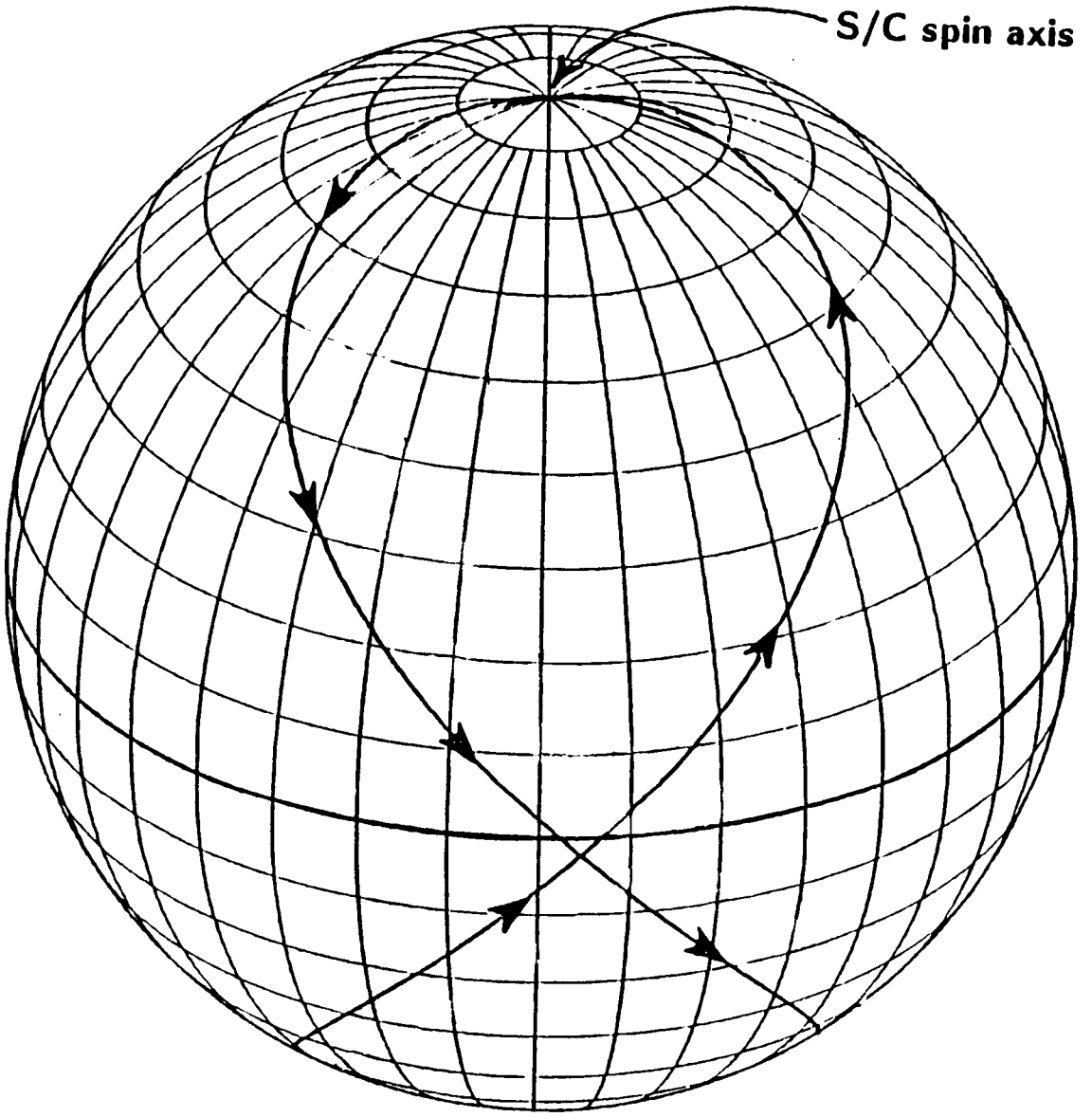

FIGURE 4.1-3
SCAN TRACE WITH SCANNER AND SPACECRAFT SPEEDS MATCHED

With the scanner spin rate exactly matched to the spacecraft spin rate, the pattern would retrace every revolution of the spacecraft. By slightly increasing the speed of the scanner, the pattern would begin to advance in space. Figure 4.1-4 shows the scan path advancing across the global sphere around the spacecraft. The resolution between one scan path and the next is strictly a function of the difference between the spacecraft spin rate and the scanner spin rate. Advancing the pattern in the opposite direction is done by simply decreasing the scanner speed so that it is slightly less than the spacecraft spin rate.

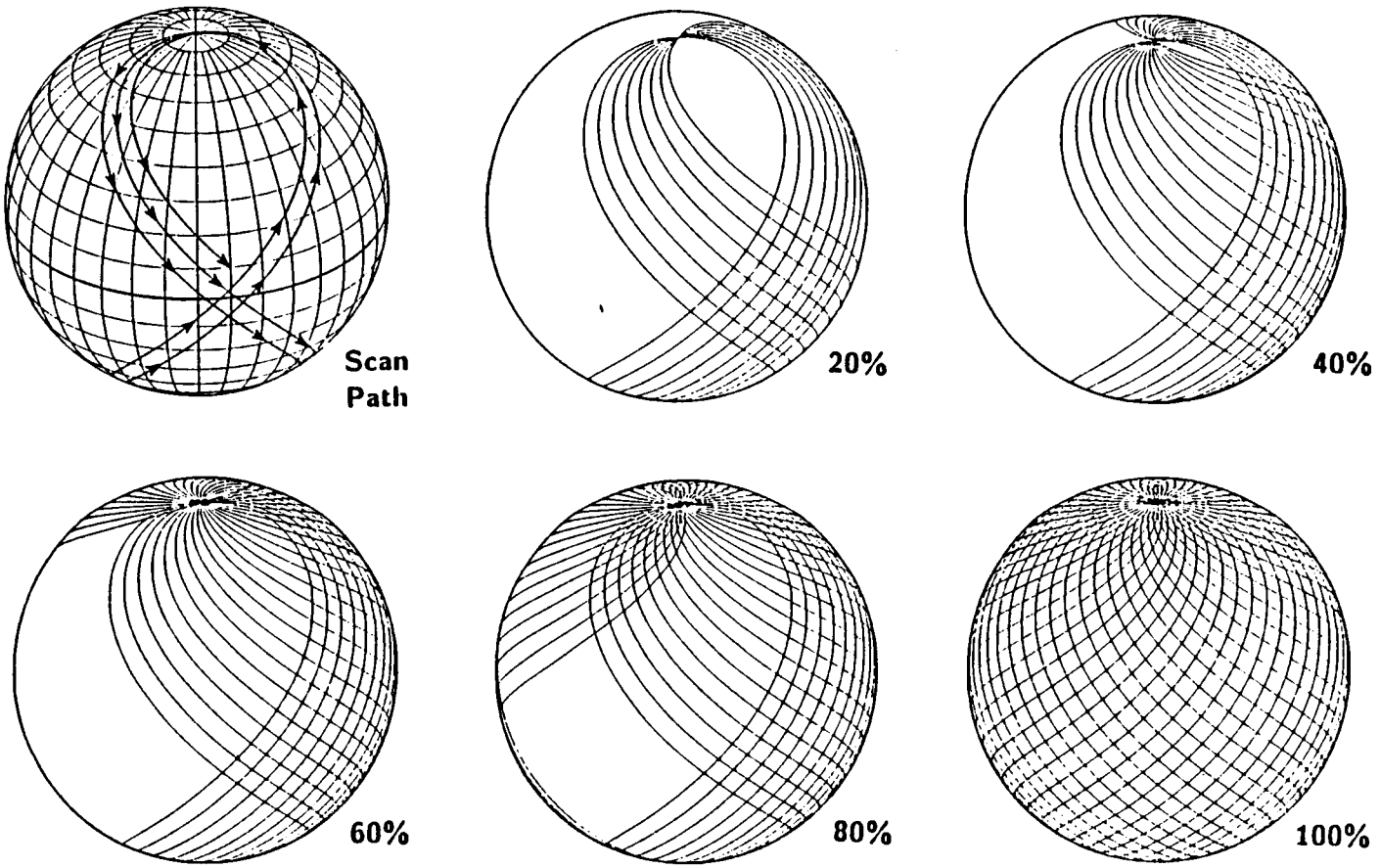

FIGURE 4.1-4
FULL-SKY COVERAGE OF SCAN TRACE

This concept produces a scanner that is highly agile. As well as straight forward control of the scan pattern's resolution, other options are available when using this scanning technique. For example, it is possible to scan at a scanning speed to spacecraft spin rate ratio of more than 1. Thus, for a specific resolution, the entire 4π steradian may be scanned in less time. Effect of multiple scan ratios are shown in Figure 4.1-5.

Though scanning the entire sky with a scanning speed-to-spacecraft spin rate ratio of 2,3,... is interesting, there does not seem to be any great advantage for doing so during the ISTP missions. Using some of the more advanced techniques presented in Section 4.6, there will be an ample amount of time to acquire data. More attention to this will be given in Phase II.

Coverage of 4π steradians is accomplished using proven sensor technology. Movement of the scan path in space is simply a function of motor speed, resulting in a highly controllable scanner. Resolution between scan paths is a function of the ability to control the motor's speed.

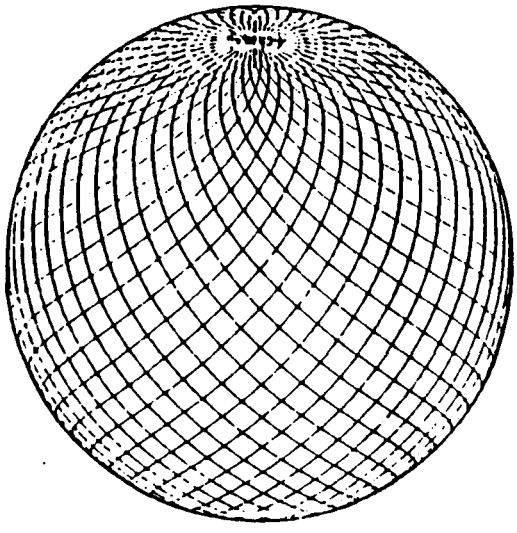

Scan: Spin = 1:1

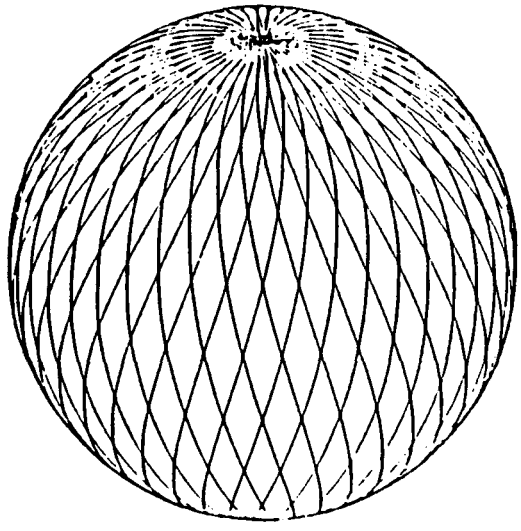

Scan: Spin = 4:1

Time to Complete Full Sky Scan

Resolution (degrees)	Sensor Head Scan Rate (rpm)		
	20	80	200
1.0	18 min	4.5 min	1.8 min
0.2	90 min	22.5 min	9 min

FIGURE 4.1-5
MULTIPLE SCAN RATES

4.2 Horizon Location

In this section the problem of accurate horizon detection of small objects is explored. This is the job the sensor must do to insure accurate centroid determination by ground processing.

Instantaneous horizon location of large objects, such as the Earth, is commonly done to accuracies of 0.1p to 0.5° at low orbits, and 0.03° at geosynchronous orbits. Our objective is to achieve 0.2° at low orbits and <0.1° at the L1 Lagrange point by reducing the effects of noise through the ground processing.

4.2.1 Worst Case Orbit

The Sun, the Earth, and the Moon are all detectable in low Earth orbit. Because the Sun is far enough away, it is for all practical purposes a constant distance from any of the orbits being considered, and will be detectable from any orbit.

For sensors designed for low-Earth orbit, the infrared optical passband is set to the 14 to 16 micron CO_2 absorption band. In this band, detected radiation comes from black-body emissions from the upper atmosphere. The atmosphere acts like a filter and prevents the sensor from seeing the ground or storms at low altitudes; also eliminating day/night effect. A considerable amount of effort has been expended over the years by NASA and others to determine characteristics of the Earth's infrared signature in this passband.

We know from past experience that we obtain ample signal from the Earth and can expect to do horizon location with no difficulty at low and moderate orbits. Thus, the area of concern is the higher orbits where the Earth is so far away that the full Earth disk is not large enough to fill the sensor field of view. In those cases, the signal levels obtained will be less than those for low-Earth orbits. Thus, the worst case is the higher orbit case, specifically the Sunward Libration point (L1).

4.2.1.1 Worst Case Earth

At the L1 libration point, the Earth is less than 0.5° wide; thus it will not fill the FOV. Figure 4.2-1 is a plot of the Earth signal resulting from a scan of the FOV across the Earth. This is the maximum signal obtainable and represents the case where the center line of the FOV passes through the center of the Earth disk. The maximum signal obtained is about 20% of a typical low-orbit Earth signal. Thus, at best we have only 20% of our normal low-orbit Earth signal level available. Similar calculations indicate that if the FOV center misses the Earth center by 0.5°, the peak signal is only 8% of a low-orbit Earth signal.

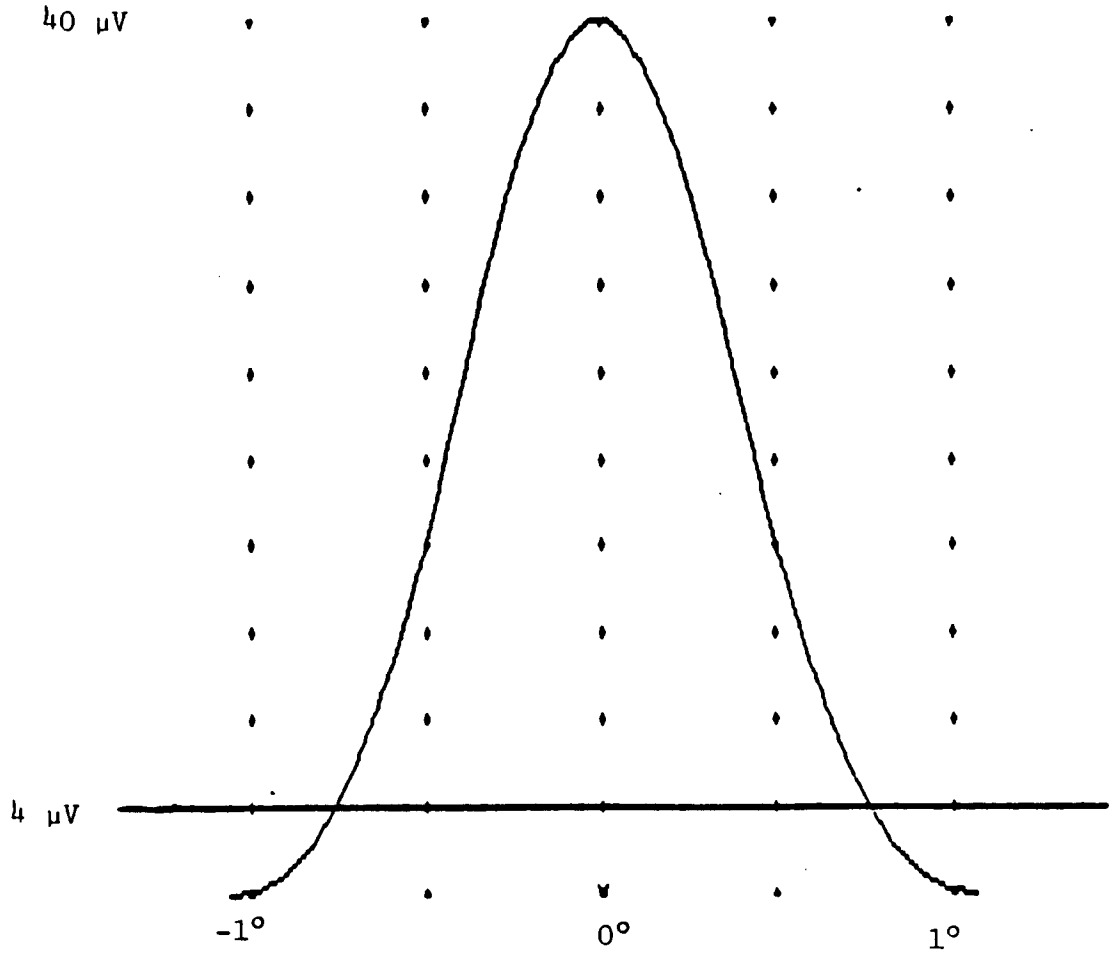

FIGURE 4.2-1
MAXIMUM EARTH SIGNAL AT L1

4.2.1.2 Worst Case Moon

The Moon has no appreciable atmosphere and a long day (14 Earth days) and night. The infrared sensor which can detect the Sun and the Earth will not see the cold side (70 Kelvin) of the Moon. Thus, unlike the Sun and the Earth, the Moon has an infrared terminator. We would expect to see emitted radiation from the Moon's surface where temperatures can vary from 390 Kelvin at the subsolar point to 70 Kelvin on the dark side[1]. The user who desires to use data from the Moon must take into account the effects of the terminator in his algorithms.

At the Sunward libration point L1, the spacecraft is located between the Sun and the Earth. The attitude cannot be determined unless the Moon is used. Fortunately, at the L1 libration point, the Moon is always fully illuminated by the Sun as viewed from the spacecraft.

From the data in the referenced report[1], an infrared model of the Moon's surface temperature distribution was defined and convolved with the FOV model to obtain signals similar to that in Figure 4.2-1. The Moon signal at its closest approach to the spacecraft peaks at 14% of a low-orbit Earth signal. At the largest separation distance, the Moon's signal is only 5% of the low-orbit Earth signal. Of course, at these two extremes, the signal is not of too much interest since the Sun, Moon, Earth, and the spacecraft will again lie approximately in a straight line. The Moon signal is of most interest when the Moon and spacecraft are at a right angle to the Earth (refer to Figure 4.2-2). In this geometry, the signal's amplitude is about 45% of the L1 Earth signal. Assuming that we wish to detect the Moon when the FOV is not directly centered on the Moon means that we would like to be able to detect the Moon signal when it is 40% of peak or about 4% of a low-orbit Earth signal. Thus, we must be able to detect a signal which is 4% of a low-orbit Earth signal in order to operate with the Moon at the L1 libration point. If we can do that, then we will also be able to find the Earth and the Sun. Furthermore, we will also be able to operate at lower orbits where signals are stronger.

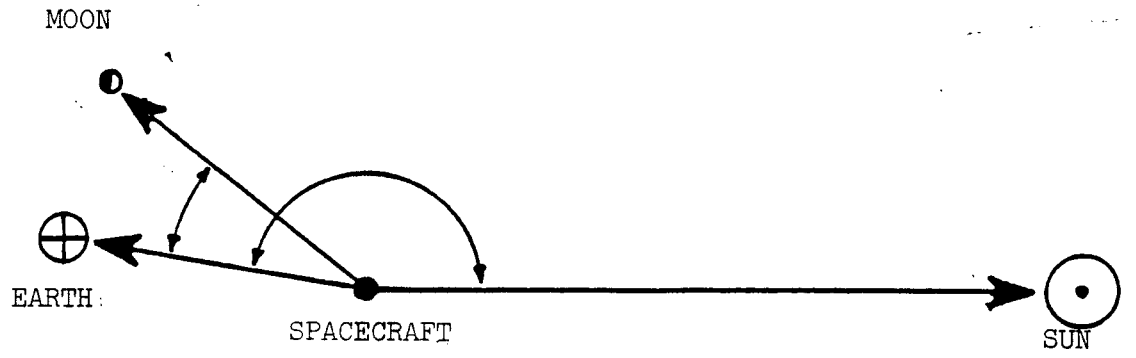

FIGURE 4.2-2
LIBRATION POINT GEOMETRY

4.2.1.3 Worst Case Sun

At the L1 libration point, we are closer to the sun than at any other orbit. However, we are only about 1% of the way from the Earth to the Sun. Thus, we have not significantly changed the Sun signal from what we are used to coping with in low-Earth orbit. A calculation of the Sun signal carried out at L1 indicates that the maximum Sun signal is 130 times a low-orbit Earth signal versus 127 times in low-Earth orbit.

The problem with the Sun is not in finding it, but in coping with it and its effects on the Earth and Moon processing electronics. A separate channel of electronics will be devoted to processing the Sun, so the actual location process devoted to the Sun can be optimized without degrading Earth/Moon performance. As far as the Earth/Moon electronics is concerned, the problem is a classical one of making an analog system recover gracefully from a high overload. The technique is well developed and consists primarily of carrying wide electronic bandwidth with ample dynamic range until a clipper can be inserted to reduce the amplitude of the overload, as described in Section 4.2.3.3.

4.2.1.4 Worst Case Summary

The worst cases for the ISTP systems are encountered at the L1 libration point. There we have to detect a signal which is 4% of the low-orbit Earth signal. At the same time, we have to cope with possible effects of a 130 times Earth signal from the Sun. The 4% requirement determines the minimum signal to noise ratio which we must achieve with the sensor. The system will have enough dynamic range to be able to operate in low-Earth orbit and on rare occasion in the neighborhood of the sunlit side of the Moon. A summary of the signal levels at the L1 libration point and at low-Earth orbit is given in Table 4.2-1.

	Low Earth Orbit	LI Libration Point (see Figure 4.2-2)
Earth	100%	8%
Moon	14% (low-lunar orbit)	4%
Sun	127 X 100%	130 X 100%

TABLE 4.2-1
RELATIVE SIGNAL AMPLITUDES

4.2.2 Optical Considerations

4.2.2.1 Optical Passband

Low-orbit horizon sensors are normally restricted to using the 14 to 16 micron band. This band minimizes the effects of atmospheric disturbances and infrared signals from the surface of the Earth or the sensor. To a certain extent, the ISTP sensors are relieved from that requirement. All of the orbits are high, ranging from 7000 kilometers out to 1.6 million kilometers at the libration point. Fine detail at the Earth's edge has little effect at these altitudes compared to the effects in low orbit. Thus, we can open the optical passband and obtain more signal by trading away some of the atmospheric stability that is required for 0.1° accuracy in low orbits.

ITHACO has built half-degree systems (Nimbus for example) that operated from 12.5 microns to beyond 17 microns. Thus, an optical passband change is certainly a viable option and will provide about three times the normal signal.

The analysis of signals and the signal-to-noise considerations presented to follow DO NOT assume that any optical passband changes have been made. These were not changed because of the vast experience ITHACO has with the present passband and the signal levels. If the sensor can be shown to operate with the present passband, then performance can only improve with the larger improved signal to noise ratios and greater margins obtainable with a wider optical passband.

4.2.2.2 Field of View

The sensor FOV is a 1.1° round field of view. That is, the FOV is approximately round and the sensor is about 50% as sensitive to signals 0.55° off axis as it is to signals on axis. Figure 4.2-3 is a cross section plot of the typical FOV used in the computer analyses that follows.

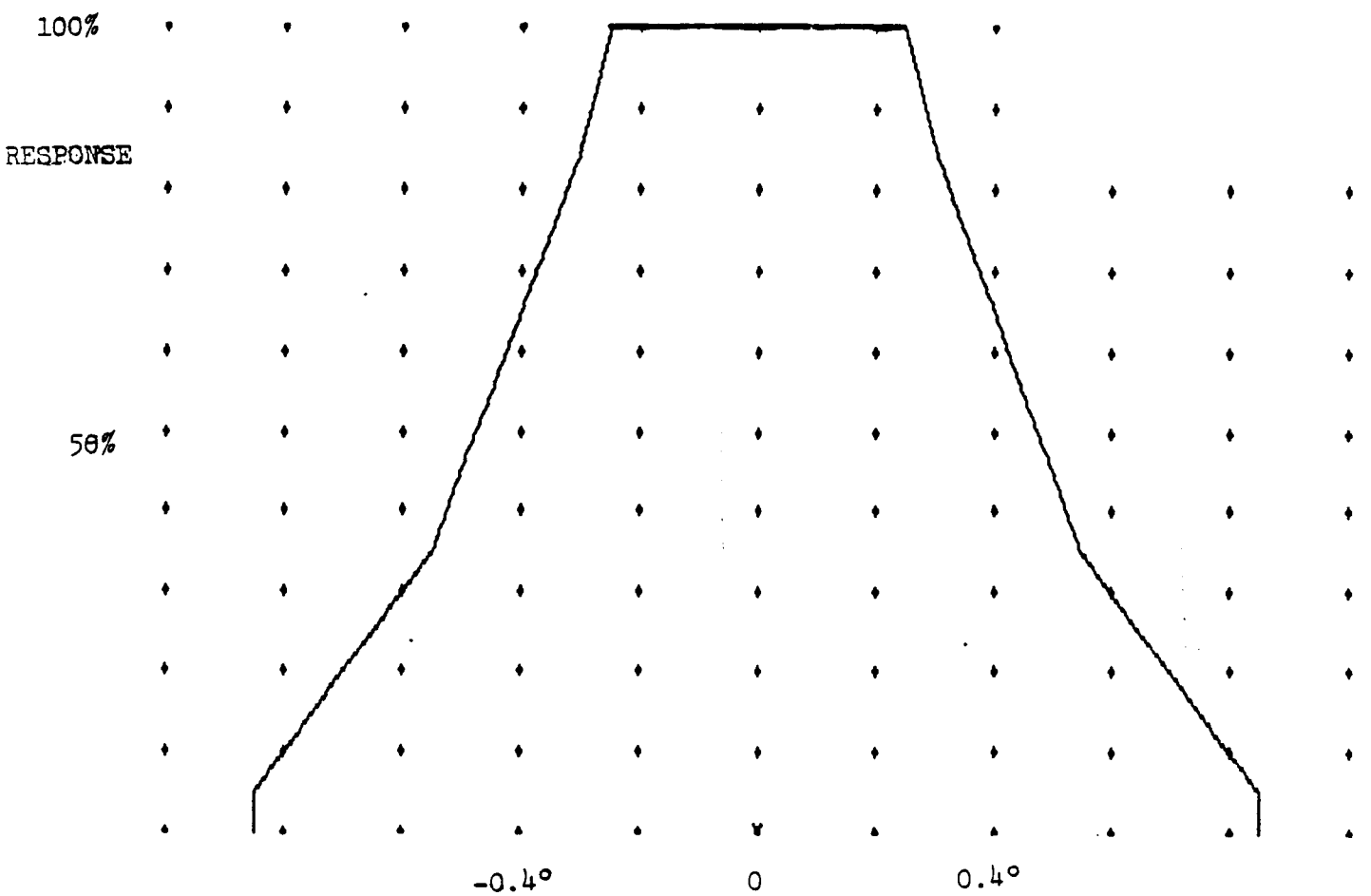

FIGURE 4.2-3
FOV CROSS SECTION

4.2.3 Locators

The term locator refers to the technique of defining the leading or trailing edge of the Earth or other celestial objects being viewed as the sensor scans through the body. This is done on the spacecraft. The term locator DOES NOT refer to the process of obtaining the centroid of the body, which is done on the ground. Determining the centroid is addressed in Sections 4.7.1 and 4.7.4.1 of this report.

4.2.3.1 Earth Locator

4.2.3.1.1 Differentiating Locator

The locator choice is driven by the signals that the horizon sensor sees from the libration point. Most recent experience with horizon sensors at ITHACO has been with the differentiating locator. A computer model of the signal processing circuits has allowed simulation studies of performance of the sensor under various conditions to be carried out. As an initial test of the difficulties of operation at the libration point, the waveform in Figure 4.2-1 was applied to the computer model. The model parameters were optimized for low-Earth orbit operation. The standard (low-orbit) rotor speed of 120 RPM was assumed. The results were far from encouraging. The differentiator output was approximately what one would expect from the impulse response of the electronics. The amplitude was so small that the signal was below minimum thresholds, the following circuits would ignore the signal.

The response of the simulated differentiating sensor indicated that if the sensor were to take reasonable data in the real world versus simply giving back the electronic impulse response, then bandwidths would have to be increased or rotor speed would have to be reduced or both. The differentiator works fine in low-Earth orbit, but the difficulties in achieving detectable signals at L1 with wide bandwidths make the locator appear unattractive. Consequently, we rejected the differentiating locator.

4.2.3.1.2 Normalizing Locator

The normalizing locator is the next logical choice. However, due to the extremely large dynamic range of signals, the normalizing locator is not practical. Thus, the normalizing detector was also rejected.

4.2.3.1.3 Fixed Radiance Locator

The simplest locator is a "fixed radiance" locator. The Earth signal is amplified, filtered, and then applied to one input of a comparator, the other input being connected to a fixed reference voltage. When the Earth signal exceeds the comparator threshold, the comparator signals that Earth is being viewed. When the Earth signal again drops below the threshold, the comparator signals that Space is being viewed. Quite satisfactory horizon sensors have been built using this simple scheme, Nimbus being a notable example. Performance is typically about 0.5° in low-Earth orbit (without ground processing).

The fixed radiance locator normally suffers from one significant error source. The precise time that the comparator detects the Earth is dependant upon the amplitude of the Earth signal. That amplitude can vary depending upon the temperature of the Earth's atmosphere. Thus, we say that the locator is radiance sensitive.

The fixed radiance locator would normally yield poor results. In this application, however, where at the L1 point the Earth is viewed in a plane that is within about 23° of the equator. The radiance changes from localized cloud patterns are largely averaged out because the Earth is smaller than the sensor field of view (FOV), and therefore, radiance variations will be substantially less at the L1 libration point than at low orbits. It would be surprising, in fact, if the variation in the average Earth temperature changes much at all when viewed from the libration point. The winter pole will not be seen, and that accounts for most of the atmospheric disruptions that affect low-orbit sensors[2]. It might even be possible to argue that if there is not a reasonably constant average radiance balance on the Earth over the period of time we have at our disposal for averaging, that this would have catastrophic consequences to all of us.

Consider Figure 4.2-4, a fixed radiance locator is shown that is set at about 10% of the maximum Earth amplitude, safely above the noise. Both the width of the Earth and the amplitude are modulated as the field of view scan path moves from being partially off the Earth to being completely on the Earth. Note that at K = 0.5°, the pulse width has changed and is at 70% of the peak Earth width, while the amplitude has dropped to 40% of the peak. This is in part due to the field of view model used (Figure 4.2-3) which approximates the bolometer detector we now use. The significance of this is that in one axis the amplitude is a more sensitive measure of the position than is the pulse width. In this other axis (along the path of the scan) it doesn't matter. We believe that a fixed locator with readout of amplitude, pulse width, and pulse phase is the optimum locator for this application.

4.2.3.2 Moon Locator

Since the Moon signal is about half that of the Earth at L1, the locator will be the same. However, this imposes scanner speed limitations as discussed in Section 4.4.

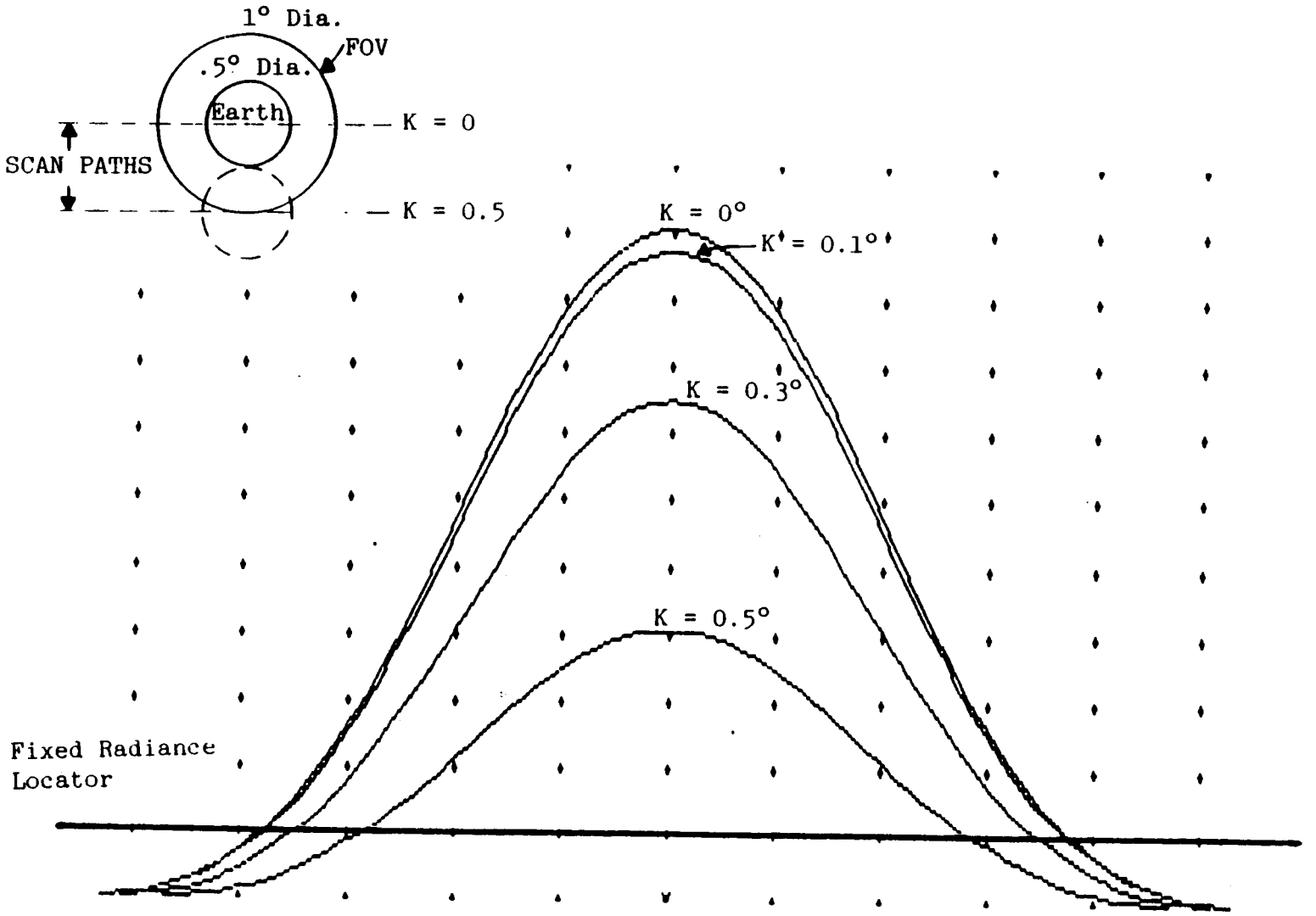

PULSE WIDTH

Pulse Width changes by 24% at K = 0.5
Amplitude changes by 40% at K = 0.5

FIGURE 4.2-4
FIXED RADIANCE LOCATOR

4.2.3.3 Sun Locator

As stated in Section 4.2.1.3, the problem with the Sun is not in finding it, but in coping with it and its effects on the Earth and Moon processing electronics. A separate channel of electronics will be devoted to processing the Sun, so the actual location process devoted to the Sun can be optimized without degrading Earth/Moon performance. As far as the Earth/Moon electronics is concerned, the problem is a classical one of making an analog system recover gracefully from a high overload. The technique is well developed and consists primarily of carrying wide electronic bandwidth with ample dynamic range until a clipper can be inserted to reduce the amplitude of the overload. Once the Sun signal has been limited, than bandwidths can be reduced commensurate with Earth/Moon requirements. The Sun signal thus gets clipped to a low level before it can disturb the electronic filtering. By clipping the Sun signal, the disturbance to the electronics is minimized. The electronics then can recover much quicker and more linearly than otherwise would be possible.

4.3 Signal-to-Noise Analysis

The low-Earth signal level achieved by our CES is about 200 microvolts at the bolometer. The optical passband is 14 to 16 microns with the 1.1° FOV and a 210° Kelvin Earth signal. We will use that signal level as our baseline. We want to be able to detect a signal which is about 4% of this level (Moon at L1). Thus, we want to be able to reliably detect an 8 microvolt signal at the L1 libration point.

The bolometer noise level is approximately the Johnson noise generated by its resistance. The two flakes are wired in parallel and, at room temperature, have a parallel resistance of about 125 kohms. The Johnson noise from a 125,000 ohm resistor is 45.5 nV/root Hz. Of course, we do not do this well in practice because of preamplifier noise and bolometer current noise effects as well as 1/f effects. Allowing another 30% for other noise sources leaves us with approximately 60 nV/root Hz as achievable performance from a bolometer. See ITHACO report #92575 Rev. A for a detailed noise analysis on a CES.[3] The preamplifier design maintains the room temperature signal-to-noise performance over a bolometer temperature span from -15°C to 25°C. Temperatures above 25°C or temperatures below -15°C degrade signal to noise performance.

In order to detect an 8 microvolt signal, the noise level must be less than 8 microvolts. Since we want to insert a threshold which is not perturbed by noise when no object is present and is not tripped by noise when the signal is present, the threshold must be at 4 microvolts. Thus, we want a peak noise level of less than 4 microvolts. This implies an RMS noise level of 4/3 microvolt. In practice, one would want some margin, so an RMS noise level of 0.8 microvolts is a reasonable goal. If we have a noise bandwidth of 175 Hz, then we should achieve the required signal to noise ratio.

$$60 \text{ nV} \times \sqrt{175} = .794 \text{ microvolts}$$

Intrinsic to the nature of a thermistor bolometer is a thermal lag. This lag is a real pole in the response of the bolometer. That lag is compensated out by a matching lead network. The lead unfortunately increases the noise bandwidth of the system and must be accounted for in the design of a filter. For our purposes, let us assume that the lead required is 2 milliseconds to compensate the detector. Then the following filter provides the requisite 175 Hz noise bandwidth.

$$f(s) = \frac{(1 + .002\,s)}{(1 + 1.162\times10^{-3}s)(1 + 1.990\times10^{-3}s + 1.258\times10^{-6}s^2)(1 + 1.085\times10^{-3}s + 989\times10^{-9}s^2)}$$

This is a five-pole Bessel filter with a 0.002 sec. lead.

4.4 Motor Speed Effect on Locator

In Section 4.1, it was shown that full-sky coverage may be completed faster, with the same resolution, by turning the scanner at multiples of the spacecraft rotation speed. In this section, the effect of scanner spin rate on the signal will be presented.

Figure 4.4-1 is a plot that shows the response of the filter described in Section 4.3, to the maximum Earth signal at the L1 libration point. The pulse centered about the X-axis "0" is the input pulse from the convolution of the FOV model and the Earth model. The calculated outputs assume either a fixed sensor with the spacecraft rotating at 20, 40, 60 or 80 RPM or conversely a fixed spacecraft with the sensor motor running at those speeds. For a running sensor motor on a spinning spacecraft, the actual equivalent speed of the FOV is higher than either, but less than the sum of both depending upon the instantaneous orientation of the FOV. For simplicity right now, we assumed constant speed. For reference, the amplitude of the Moon signal (45% of the Earth signal) is noted.

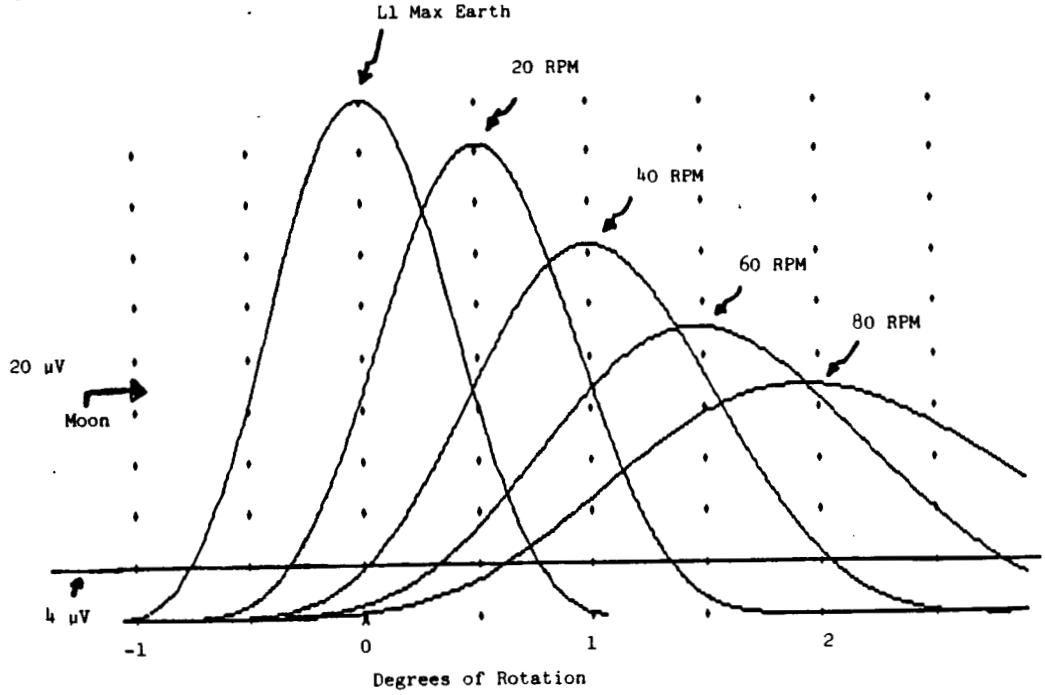

FIGURE 4.4-1
FILTER RESPONSE TO EARTH PULSE AT 20-80 RPM SCAN SPEED

The filter closely matches what would be expected from a Bessel design. The input pulse shape is well preserved. The output pulse closely resembles the input pulse delayed by a constant time delay. The plot X axis is in scan degrees, not time which is why the peaks shift to the right as the speed increases.

At the lowest speed plotted, the output signal peaks at 90% of the input signal. Thus, we have managed to get most of the signal through the filter and the detection process will be quite solid. In fact, the detection process is quite solid even at 80 RPM for Earth detection. This means that we will be able to find the Earth at these speeds. The peak output versus input is tabulated below.

Speed (RPM)	Peak output (%)	Peak output (microvolts)
20	90	36
40	73	29
60	55	22
80	45	18

In Section 4.2.1.1, we determined that we wanted to detect the Earth when we missed the center of the Earth by 0.5° with the FOV. The Earth input signal then would be 16 microvolts. At 60 RPM then, the filter output signal would be 8.8 microvolts and reliable detection would still be possible. Thus, on a 20 RPM spacecraft, running the sensor motor at 40 RPM provides reliable Earth data.

The peak Moon that we expect is 18 microvolts because of the smaller size of the Moon. See Section 4.2.1.2. By the same reasoning, we could detect the Moon then with a rotor speed of 40 RPM. However, if we miss the Moon by 0.5°, then we would expect the Moon signal to also be attenuated to 40% of peak as in the case of the Earth. In this case, the Moon signal would be 7.2 microvolts and on the borderline of detectability even with a scan speed lower than 20 RPM which is not available. Thus, we can find the Moon at 40 RPM, but must hit it quite closely to do so. Since the actual FOV speed is a function of both the spacecraft rotation speed and the sensor motor speed, actually running the motor at 40 RPM would make detecting the Moon questionable except when the FOV crosses very close to the middle of the Moon. Thus, we should expect to run the sensor motor at the same speed as the spacecraft is rotating when we are looking for the Moon at the L1 libration point.

Here is where increasing the optical passband could help. If we were to approximately double the throughput of the optics by increasing the optical bandwidth, then the Moon detection problem becomes comparable to the Earth detection situation discussed above.

4.5 Telemetry Interface

Actually determining the attitude of the spacecraft will be performed on the ground. The telemetry information required to determine attitude is the location of the in-crossing and out-crossings of the Earth, Sun and Moon relative to the Sun in spacecraft coordinates. Also as described in Section 4.2, the magnitude of the pulse can also be available for telemetry.

This data may be transmitted in real time as a large quantity of Sun pulses and tack pulses along with the output of the locator. Though this appears to be the simplest method, the reality would be somewhat more difficult. This system would require multiple channels to detect motor position pulses, Sun pulses, and location pulses.

A much simpler method of handling the telemetry data is by sending a digital word that contains in-crossing and out-crossing information. This information may be simply obtained by tracking the positions of the motor and the spacecraft. When an in-crossing or out-crossing is detected, the position of the motor and spacecraft is stored in a register. The motor position may be measured directly off the motor's code wheel (tack track). The rotational position of the spacecraft may be measured by timing the interval between the Sun pulse and the location of the in-crossing or out-crossing. The only additional information required is the spin rate of the spacecraft. This is obtained by measuring the time from one Sun pulse to the next.

Figure 4.5-1 shows the interconnecting of the inputs to produce the telemetry required for attitude and position determination. The output of the Adcole Sun sensor is fed into the counter/latch control. This would perform two tasks. First, it would latch the current number in counter A into latch A. Second, it would reset the counter in some constant, and preferably negligible, time after latching A. The counter would then start counting as a function of the oscillator. At the next Sun pulse the above two tasks would be repeated. Note that the number in latch A is a function of the time between Sun pulses. That is, the spacecraft spin rate may be calculated from the number in latch A given that the frequency of the oscillator is known.

The locator produces a signal when an in-crossing or out-crossing is detected by the sensor. When an in-crossing is detected counter A would be stored in Latch B. The time between a Sun pulse and the detection of an in-crossing can be determined from the number in latch B. The same applies for the out-crossing using latch C. With the knowledge of the spin rate of the spacecraft and the time from a Sun pulse to a crossing the rotational position of the spacecraft is known with respect to the Sun at the event.

If the output of the motor tack increments a second counter (B) and the counter is reset by a commutator (probably along a spin axis), then counter B tracks the position of the motor. Latches D and E then store the position of the motor at the time of the location of the in and out crossings.

Latch F stores the rotation time of the motor. Thus, the average motor speed is known.

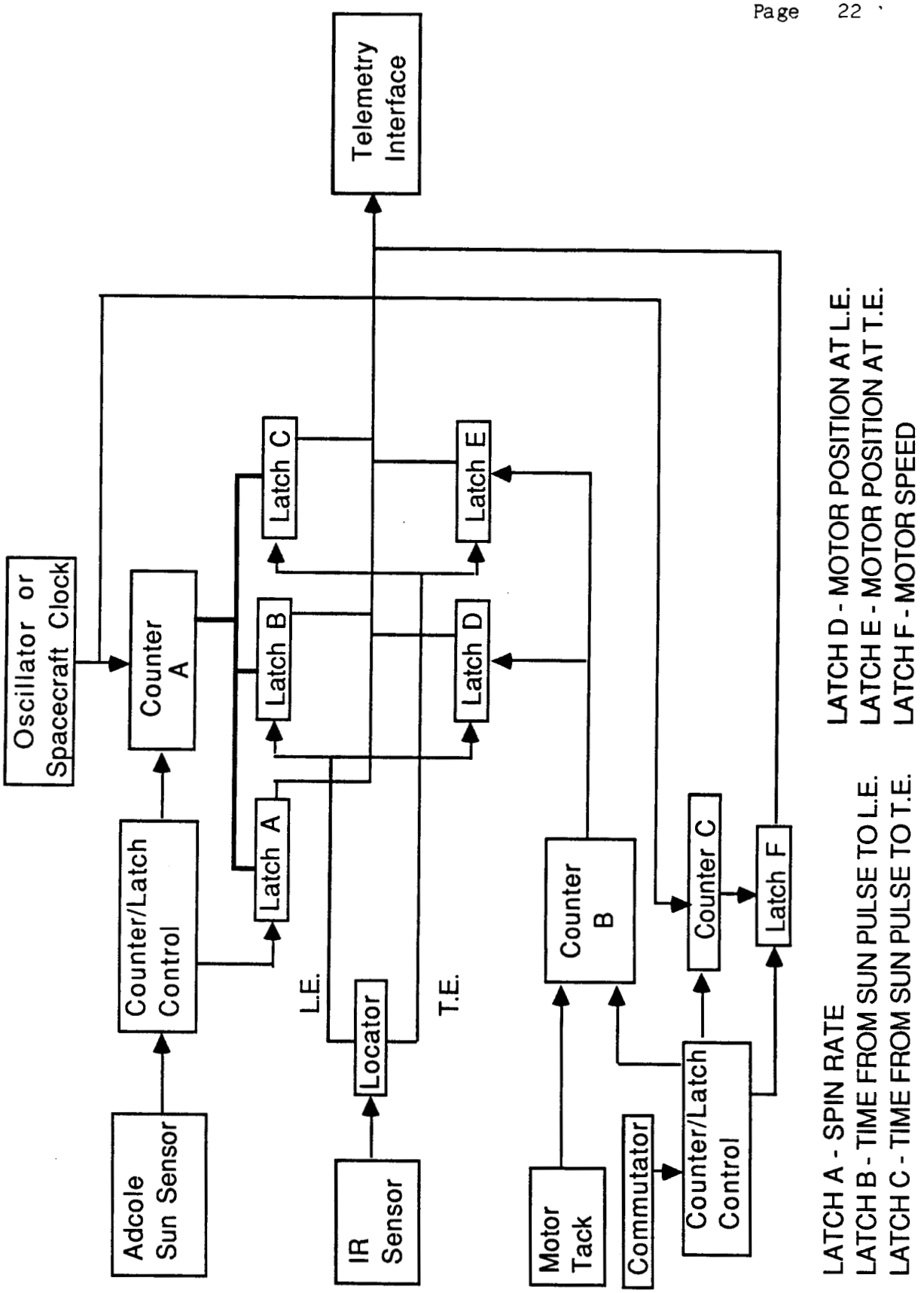

FIGURE 4.5-1
BLOCK DIAGRAM OF DATA GENERATION ELECTRONICS

The resolution of the motor tack itself may not be sufficient to locate the position of the motor to the required tolerance. By synthesizing pulses in between the tack track signals, the resolution required can be obtained. The synthesized pulses may be produced as follows:

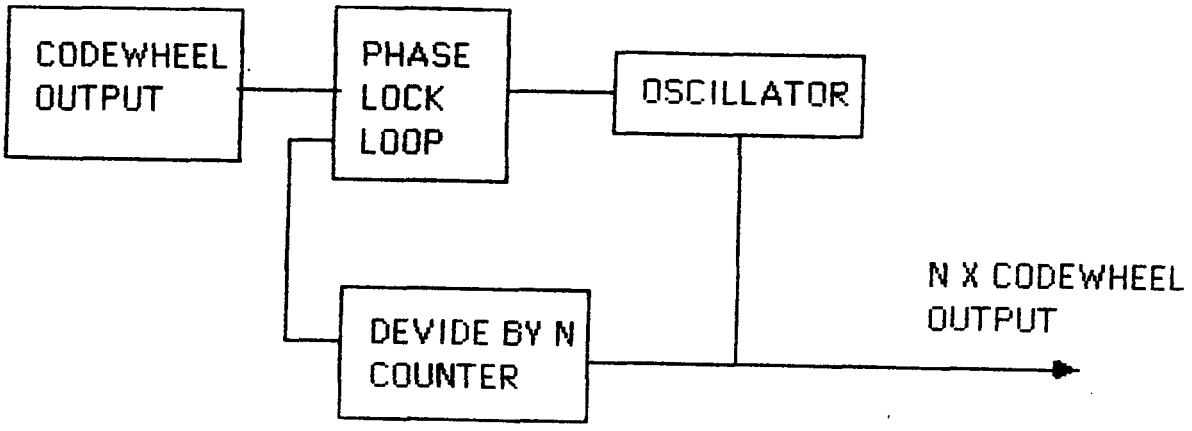

FIGURE 4.5-2
FREQUENCY MULTIPLICATION SCHEME

A tape recorder is available to transmit whenever required. Data would only be transfered to the tape machine when an object is viewed. The tape machine would store the data until the ground requests that the data be telemetered down to earth.

4.6 Operating Modes and Command/Telemetry Requirements

4.6.1 Autonomous Mode

The FSS must be able to operate over a period of days without intervention from the ground. Thus, an automatic mode must be defined. The simplest auto mode would continue to scan out the entire sky with 0.2° resolution between scan traces. As an object is observed, the in-crossing and out-crossing data would be generated and transferred to the tape recorder.

At 0.2° steps it would take 1800 revolutions to scan the sky. At 10 RPM (6 seconds per revolution) it would take 180 minutes to complete one scan. Therefore, in one day it would complete 8 scans of the entire sky. The Moon has a viewable width of 0.8° when viewed at the L1 Lagrange point. Therefore, the maximum number of data pairs per sky scan would be 4. In 24 hours only 20 data pairs would be obtained. Recorded data may only be available for 6 hours after the original transmission. Thus, only 5 data pairs would be saved. It is desirable to have more data available for attitude determination.

An alternative to the simple scan mode described above would be to start off in a search mode. The search mode must be fine enough to guarantee finding the Moon at L1. With a viewable width of 0.8° the search mode should be approximately 0.5° resolution.

Once an object is observed, the scanner will switch to an ultra fine mode. As the scanner leaves the object, the motor speed can then be readjusted to cause the scanner to sweep back over the object. This process may be repeated as required to achieve a sufficient amount of data. The more data obtained, the better the results will be due to the nature of the least squares fit performed during the ground processing.

Further time may be saved by "remembering" the location of the Earth, Sun and Moon. Large areas in space that contain no targets may be quickly skipped to home in on the areas of interest. This technique would provide massive amounts of data in relatively short periods of time.

4.6.2 Ground Control Mode

If the telemetry information can be transmitted, rather than recorded, as soon as the data is generated, then many possibilities exist for real time control of the sensor from the ground. By transmitting motor speed along with spacecraft spin rate, total flexibility of control is obtained. Besides the in-crossing and out-crossing telemetry data required for attitude determination, motor speed and spacecraft spin rate could be telemetered. Given this data, any portion of the sky may be scanned as required. Large amounts of data may be generated on a specific target in a relatively short period of time.

4.7 Ground Processing

Attitude determination will be performed on the ground using the telemetry data. The telemetry data locates the position of the in-crossings and out-crossings of the Earth, Sun and Moon in spacecraft coordinates. Location of the center of each body is the first step when determining the attitude of the spacecraft. Given the position of the centroids, the attitude may be determined by comparing the observed position with ephemeris positions.

4.7.1 Centroid Determination - General Overview

All the information to locate the Sun, Earth and Moon in spacecraft coordinates will be contained in the telemetry signal. In order to locate the rotational position of an object, with respect to the Sun, the telemetry data will contain the number of timing pulses between the Sun pulse and the in-crossing, the Sun pulse and the out-crossing and between one Sun pulse and the next. Thus, the time from the Sun pulse to the in-crossing and out-crossings are known and the rotational velocity is known. Determining the rotational position of the target then becomes a trivial matter.

The coelevation angle of the in-crossing and out-crossing is determined by the position of the motor at the time of the event. This information is obtained by counting the number of tick marks on the code wheel from some origin (probably pointing along the spin axis). Finer resolution may be required than supplied by the code wheel. If this is the case synthesized pulses will be supplied as discussed in Section 4.5.

Solution by least squares yields centroid position in sensor coordinates. Figure 4.7-1 shows an example of how a circle would be fit to in-crossings and the out-crossings data.

Error in center determination is decreased by virtue of a large number of data points. Thousands of data points may be easily gathered during a 6-hour period to produce extremely accurate results.

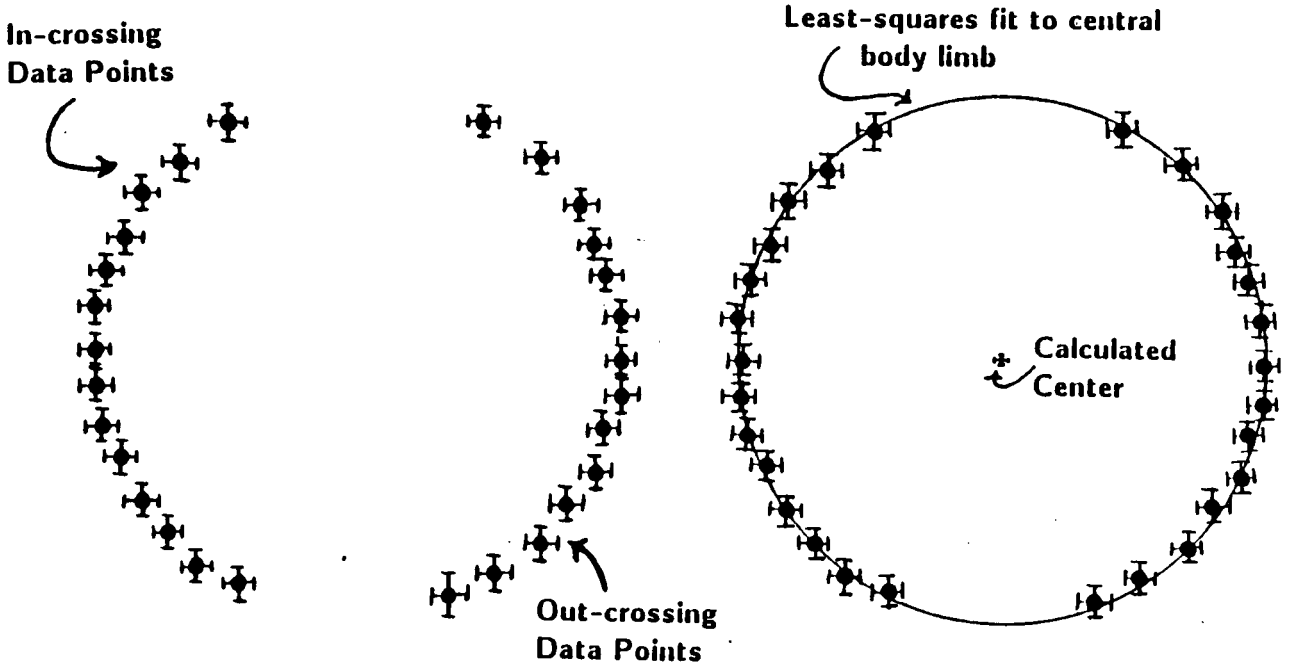

FIGURE 4.7-1
CENTROID DETERMINATION FROM IN-CROSSING AND OUT-CROSSING DATA

4.7.2 Correction for the Lunar Terminator

Determination of the centroid of the Moon will require special processing when the terminator is significant. As the terminator reduces the amount of the moon that is illuminated, the best-fit circle will also reduce in size while centering on the illuminated part of the Moon. The result will be an error in the direction opposite that of the terminator. To correct for this error a knowledge of the angle formed by the Sun, the Moon and the spacecraft, and the angular radius of the Moon is all that is required. It may be necessary to first determine the position of the spacecraft neglecting the effects of the terminator, then repeat the process after factoring in the error.

Figure 4.7-2 displays the geometry involved. The offset "d" is calculated as follows:

$$d = \frac{8\rho_{actual}\,\mathrm{Sin}^2\,(\theta/2)}{3\pi}$$

where: θ is the angle between Sun and spacecraft.
ρ is the angular radius of the Moon.

As an example, at low earth orbit:

$$\rho = 0.25^\circ,\ \theta = 90^\circ$$

Solving for d, we find that the error is 0.1° for the quarter Moon.

The terminator will only be significant at low Earth orbits. At L1, the spacecraft is between the Sun and the Moon. Thus, only the day side can be scanned and no correction will be necessary.

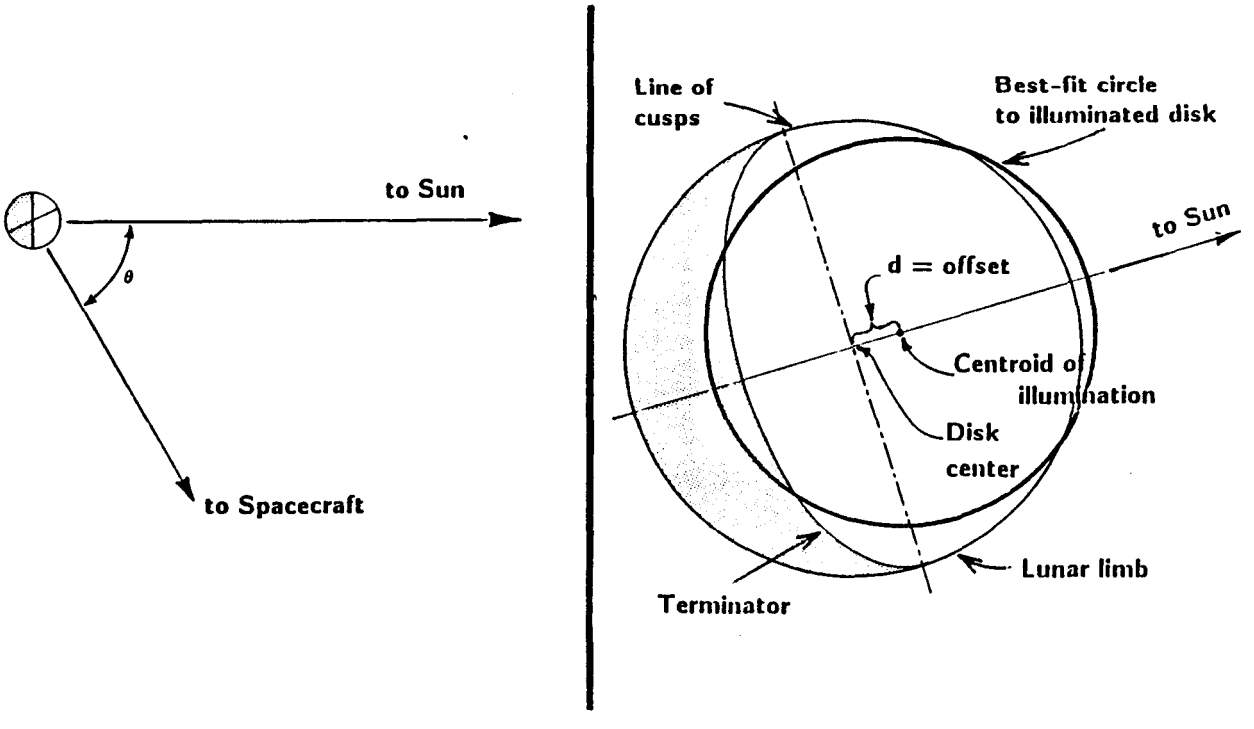

FIGURE 4.7-2
CORRECTION FOR LUNAR TERMINATOR

4.7.3 Attitude Determination

The Earth, Sun and Moon positions may be sensed anywhere in the spacecraft sky. Six independent components are immediately available. When the spacecraft is at low-Earth orbit, the diameter of the Earth is also a usable component. This data provides more than enough information to determine the spacecraft attitude.

4.7.3.1 Attitude Geometry

Each body's position may be determined in spacecraft coordinates as a function of the rotational angles about the spin axis and coelevation angles (from the spin axis to the bodies center). Refer to Figure 4.7-3 for a global geometry view of the attitude determination problem.

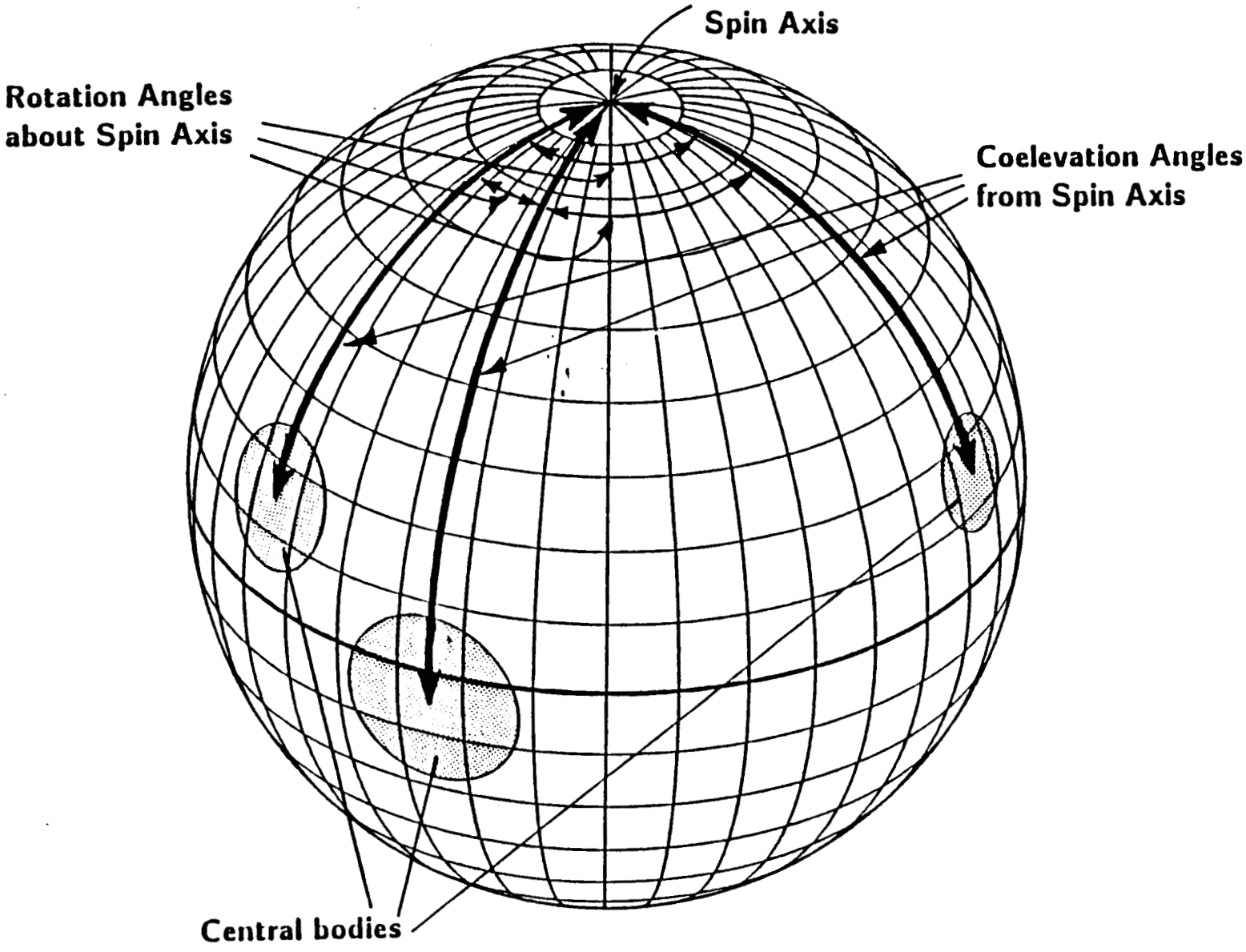

FIGURE 4.7-3
GLOBAL GEOMETRY VIEW OF ATTITUDE DETERMINATION PROBLEM

The coelevation angle to an object defines a cone on which the spacecraft spin axis must lie. On a global sphere about spacecraft, the cone would be represented as a circle. An example is shown in Figure 4.7-4. Here, solution A represents the possible attitudes of the spacecraft from the coelevation angle to the Sun. Solution B represents the possible attitude of the spacecraft from the coelevation angles to the Earth.

The interjection of the two circles define two possible attitudes. The rotational angles resolve the problem producing a unique attitude.

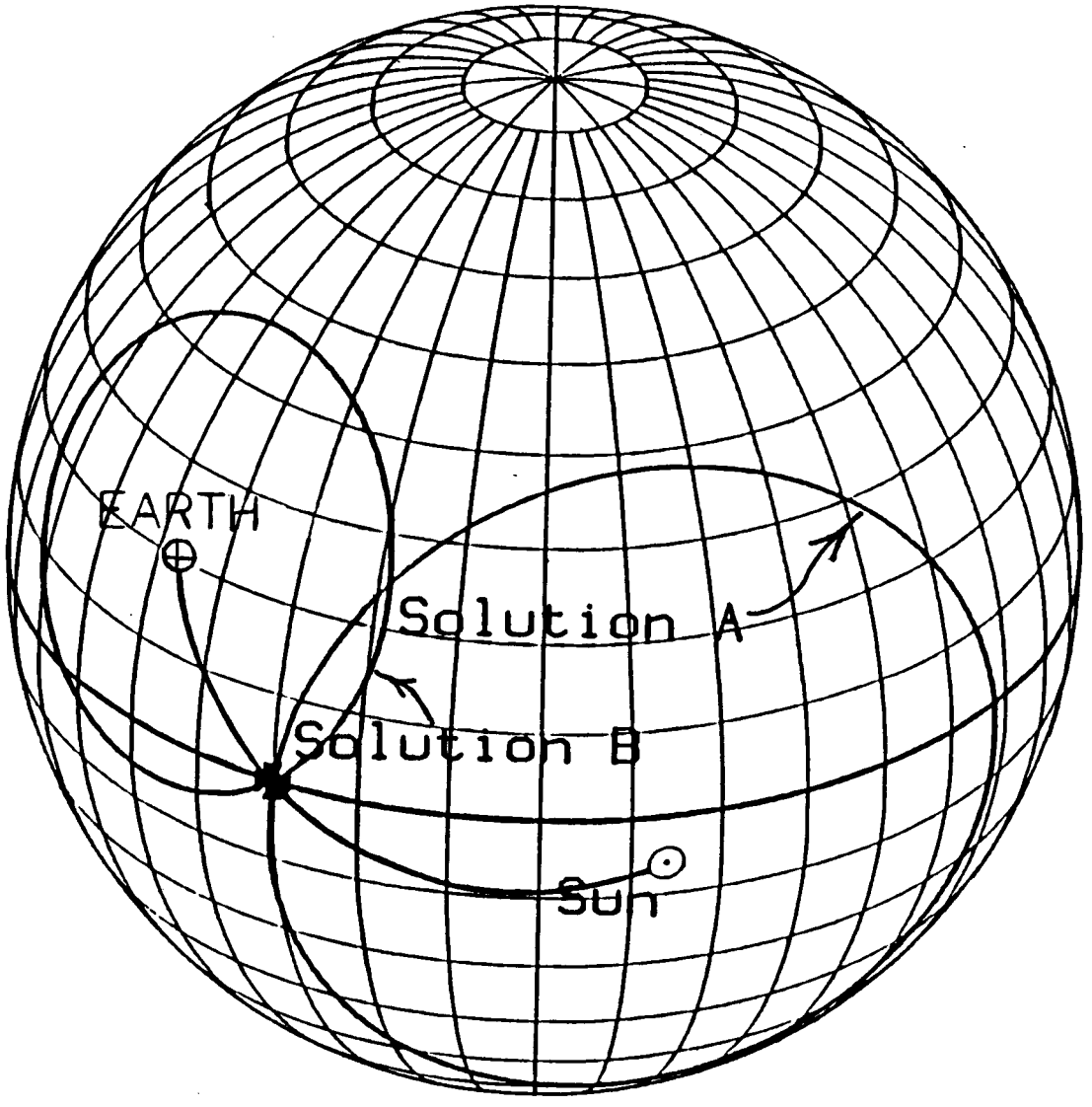

FIGURE 4.7-4
USING ROTATIONAL ANGLE TO RESOLVE ATTITUDE PROBLEM

4.7.3.2 Geometry of EQUATOR Mission

In the previous example, the use of the rotational angle was useful for resolving the two possible solutions. However, in the EQUATOR Mission the use of the rotational angle is even more important due to the geometry involved. The geometry for the EQUATOR Mission is presented in Figure 4.7-5.

In the EQUATOR Mission, the spacecraft's spin axis is nearly co-planer with the Earth and Sun. With this attitude, the loci of coelevation measurements are nearly tangent. It is difficult to accurately determine the intersection of nearly tangent circles; thus, without the rotation angle, a singularity exists that will produce poor attitude results. The rotation angle provides a measurement nearly orthogonal to the position angle measurements; thus the singularity is resolved.

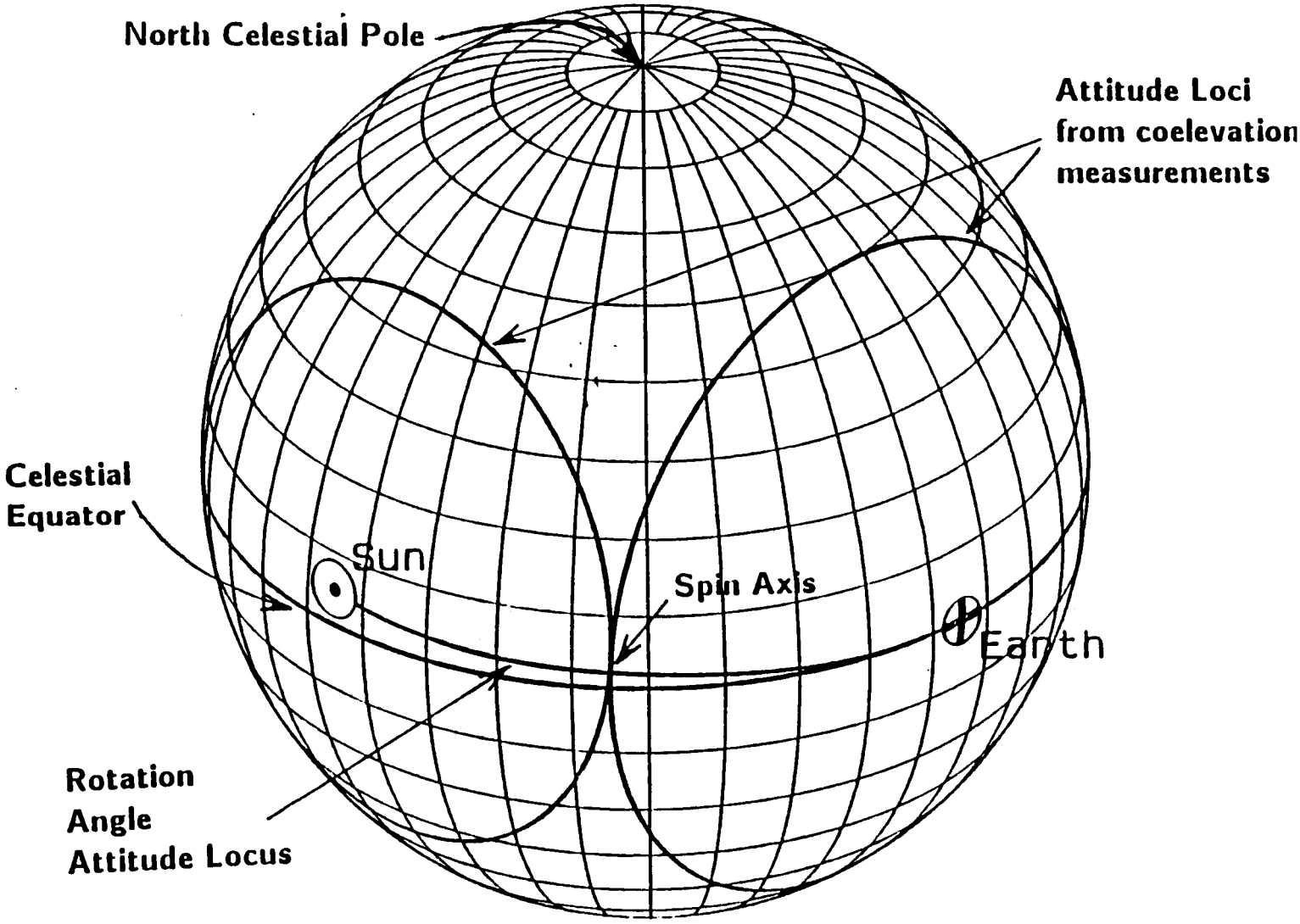

FIGURE 4.7-5
GEOMETRY OF EQUATOR MISSION

4.7.3.3 Geometry of WIND Mission

The most difficult attitude geometry exists for the WIND Mission. During this mission, the spacecraft is positioned about L1. The angle between the Earth and the Sun is 176°, or nearly colinear. Refer to Figure 4.7-6.

With only the Sun and the Earth, accurate attitude determination would be impossible. By locating the Moon, accurate attitude determination is achievable.

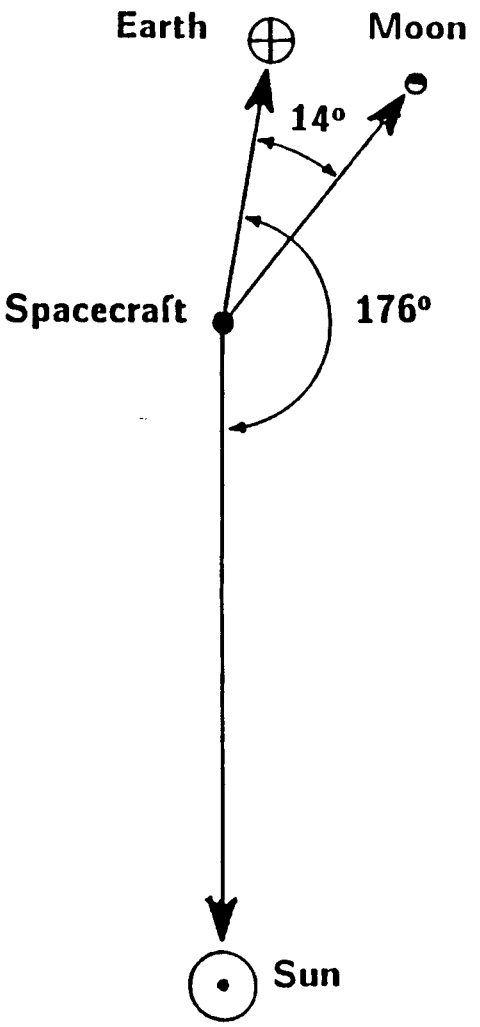

FIGURE 4.7-6
GEOMETRY OF WIND MISSION

4.7.4 Algorithms - Centroid and Attitude Determination

The algorithms presented here perform the following functions: 1) Observations are gathered for each central body and the direction to the centroid of the bodies in sensor coordinates is determined, 2) These sensed positions of the central bodies are compared to ephemeris positions and the attitude matrix is computed using methods of least-squares.

The problem falls naturally into 2 major calculations. First, a general method for finding the centroid of an object is presented (Earth, Sun or Moon for instance). Secondly, the determination of the attitude matrix from the comparison of observed and ephemeris positions is addressed.

4.7.4.1 Centroid Calculation

An observation $\hat{x}_o$ will be defined here as a sensor line of sight direction at the time of limb crossing for a central body. The centroid position $\hat{x}_c$ is the direction to the center of the central body. Both $\hat{x}_o$ and $\hat{x}_c$ are expressed in sensor coordinates. The dot product of $\hat{x}_o$ and $\hat{x}_c$ is equal to the cosine of the central body angular radius, RHO. In component form this may be written as:

$$x_o x_c + y_o y_c + z_o z_c = \cos\,(RHO)$$

This equation is for a single observation. Typically, there are many observations over the disk of a celestial object. For n observations over a given central body, a set of n equations may be written for the unknown x_c, y_c, z_c and RHO. In matrix

$$\begin{vmatrix} x_{o1} & y_{o1} & z_{o1} \\ x_{o2} & y_{o2} & z_{o2} \\ x_{o3} & y_{o3} & z_{o3} \\ \vdots & \vdots & \vdots \\ x_{on} & y_{on} & z_{on} \end{vmatrix} \begin{vmatrix} x_c \\ y_c \\ z_c \end{vmatrix} = \cos(RHO) \begin{vmatrix} 1 \\ 1 \\ 1 \\ \vdots \\ 1 \end{vmatrix}$$

dividing both sides by the scalar cos(RHO) we obtain:

$$\begin{vmatrix} x_{o1} & y_{o1} & z_{o1} \\ x_{o2} & y_{o2} & z_{o2} \\ x_{o3} & y_{o3} & z_{o3} \\ \vdots & \vdots & \vdots \\ x_{on} & y_{on} & z_{on} \end{vmatrix} \begin{vmatrix} x_c/\cos(RHO) \\ y_c/\cos(RHO) \\ z_c/\cos(RHO) \end{vmatrix} = \begin{vmatrix} 1 \\ 1 \\ 1 \\ \vdots \\ 1 \end{vmatrix}$$

Because the above represents n equations for three unknowns, the system is overdetermined for n>3. (Realize x_c, y_c and z_c constitute a unit vector, hence a third component may be solved for if the other two are known). The method of least-squares must be invoked to determine a best-fit for $\hat{x}_c$ and cos(RHO). To solve the $\hat{x}_c$/cos(RHO) multiply both sides of the above matrix equation by the transpose of the left-most matrix. Written out the result of this matrix multiplication is:

$$\begin{vmatrix} \Sigma x_o^2 & \Sigma x_o y_o & \Sigma x_o z_o \\ \Sigma x_o y_o & \Sigma y_o^2 & \Sigma y_o z_o \\ \Sigma x_o y_o & \Sigma y_o z_o & \Sigma z_o^2 \end{vmatrix} \quad \begin{vmatrix} x_c/\cos(RHO) \\ y_c/\cos(RHO) \\ z_c/\cos(RHO) \end{vmatrix} \quad = \quad \begin{vmatrix} \Sigma x_o \\ \Sigma y_o \\ \Sigma z_o \end{vmatrix}$$

To solve this system for the column vector $\hat{x}_c$/cos(RHO), we need only invert the 3 x 3 matrix on the left matrix and multiply the right hand side of the equation by the result of the inversion. Notice the 3 x 3 matrix and RHO of the equation is composed only of observations. The sums in the matrix equation may be formed as observations are gathered, so only 12 storage locations are needed rather than the 3n locations required if the full set of observations were stored. Also, the matrix to be inverted is symmetric and positive-definite. Because of this, very compact methods for matrix inversion may be employed. Using an IBM PC with a compact scheme we wrote, we found we could invert a 3 x 3 symmetric, positive-definite matrix in less than 0.02 seconds. Once the equation is solved for the vector x_c/cos(RHO), the angular radius may be found by:

$$RHO = \text{arcsecant} \left(\hat{x}_c/\cos(RHO) \right)$$

The unit vector $\hat{x}_c$ is found by multiplying $\hat{x}_c$/cos(RHO) by cos(RHO).

4.7.4.2 Attitude Matrix Computation

By finding the x_c's for the m central bodies, we are now in a position to calculate the attitude matrix. It is clear that typically m = 2 or 3 for all-sky scanners sensing the Earth, Sun and Moon, but here we will be general and consider m observable central bodies.

From Spacecraft Attitude Determination and Control the attitude matrix is defined as the matrix that transforms inertial positions into body-fixed coordinates. Specifically, for column vectors $\hat{x}_c$ and $\hat{x}_e$ representing a direction expressed in body-fixed and inertial coordinates respectively, their relationship through the attitude matrix A is:

$$A\hat{x}_e = \hat{x}_c \quad \text{and} \quad A^T\hat{x}_c = \hat{x}_e$$

Subscripts refer to central body in body-fixed coordinates (c) and central body positions found from an ephemeris (e). If $\hat{x}_c$ and $\hat{x}_e$ are expressed as row vectors, their relationship through the attitude matrix is:

$$\hat{x}_e A^T = \hat{x}_c \quad \text{and} \quad \hat{x}_c A = \hat{x}_e$$

The problem at this point is to determine A (or A^T) given the sets of m $\hat{x}_c$ and $\hat{x}_e$ positions. It really makes no difference whether A or A^T is calculated; therefore solve for A. Writing out the m equations relating the $\hat{x}_c$ and $\hat{x}_e$ we have:

$$\begin{vmatrix} x_{c1} & y_{c1} & z_{c1} \\ x_{c2} & y_{c2} & z_{c2} \\ X_{c3} & y_{c3} & z_{c3} \\ \cdot & \cdot & \cdot \\ \cdot & \cdot & \cdot \\ \cdot & \cdot & \cdot \\ x_{cm} & y_{cm} & z_{cm} \end{vmatrix} \quad \begin{vmatrix} A_{11} & A_{12} & A_{13} \\ A_{21} & A_{22} & A_{23} \\ A_{31} & A_{32} & A_{33} \end{vmatrix} = \begin{vmatrix} x_{e1} & y_{e1} & z_{e1} \\ x_{e2} & y_{e2} & z_{e2} \\ x_{e3} & y_{e3} & z_{e3} \\ \cdot & \cdot & \cdot \\ \cdot & \cdot & \cdot \\ \cdot & \cdot & \cdot \\ x_{em} & y_{em} & z_{em} \end{vmatrix}$$

By letting the m x 3 matrices of body-fixed positions and ephemeris positions be written as C and E respectively, the above equation can be written as:

$$CA = E$$

To find the least squares solution of A, first multiply both sides of the equation by C^T:

$$C^T CA = C^T E$$

Writing out the previous equation to illustrate the similarity between this half of the attitude determination problem with the first half:

$$\begin{vmatrix} \Sigma x_c^2 & \Sigma x_c y_c & \Sigma x_c z_c \\ \Sigma x_c y_c & \Sigma y_c^2 & \Sigma y_c z_c \\ \Sigma x_c z_c & \Sigma y_c z_c & \Sigma z_c^2 \end{vmatrix} \quad \begin{vmatrix} A_{11} & A_{12} & A_{13} \\ A_{21} & A_{22} & A_{23} \\ A_{31} & A_{32} & A_{33} \end{vmatrix} = \begin{vmatrix} \Sigma x_c x_e & \Sigma x_c y_e & \Sigma x_c z_e \\ \Sigma y_c x_e & \Sigma y_c y_e & \Sigma y_c z_e \\ \Sigma z_c x_e & \Sigma z_c y_c & \Sigma z_c z_e \end{vmatrix}$$

As before, invert a 3 x 3 symmetric, positive-definite matrix and perform matrix multiplication.

4.7.4.3 Summary of Algorithms

What follows is a brief summary of a method for determining the spacecraft attitude from full-sky sensor measurements.

For each central body solve the following system:

$$\begin{vmatrix} x_c/\cos(RHO) \\ y_c/\cos(RHO) \\ z_c/\cos(RHO) \end{vmatrix} = \begin{vmatrix} \Sigma x_o^2 & \Sigma x_o y_o & \Sigma x_o z_o \\ \Sigma x_o y_o & \Sigma y_o^2 & \Sigma y_o z_o \\ \Sigma x_o z_o & \Sigma y_o z_o & \Sigma z_o^2 \end{vmatrix}^{-1} \begin{vmatrix} \Sigma x_o \\ \Sigma y_o \\ \Sigma z_o \end{vmatrix}$$

Separate out the cos(RHO) from x_c and obtain unit vectors to the m central bodies.

Once the directions to the central bodies have been found in body-fixed coordinates, solve the following matrix equation:

$$\begin{vmatrix} A_{11} & A_{12} & A_{13} \\ A_{21} & A_{22} & A_{23} \\ A_{31} & A_{32} & A_{33} \end{vmatrix} = \begin{vmatrix} \Sigma x_c^2 & \Sigma x_c y_c & \Sigma x_c z_c \\ \Sigma x_c y_c & \Sigma y_c^2 & \Sigma y_c z_c \\ \Sigma x_c z_c & \Sigma y_c z_c & \Sigma z_c^2 \end{vmatrix}^{-1} \begin{vmatrix} \Sigma x_c x_e & \Sigma x_c y_e & \Sigma x_c z_c \\ \Sigma y_c x_e & \Sigma y_c y_e & \Sigma y_c z_e \\ \Sigma z_c x_e & \Sigma z_c y_c & \Sigma z_c z_e \end{vmatrix}$$

In the first equation of this section each of the $\hat{x}_c/\cos(RHO)$ vectors found for the m central bodies are seen to be dependent only on the observations. In the last equation the attitude matrix is seen to depend on the m central body directions in body-fixed coordinates and their ephemeris positions.

4.8 Bias Determination

Only one sensor is required to achieve accurate attitude determination; however a second sensor will provide redundancy for reliability purposes. An added benefit of the second sensor is the ability to eliminate bias error due to misalignment between the true spacecraft spin axis and the sensor.

The FSS produces two sets of scans on an object, one set from each side of the spacecraft. The error between the two centroids derived from the two sets of data, is twice the bias due to misalignment between the true spacecraft spin axis and the sensor.

Referring to Figure 4.8-1, it is clear that one sensor may resolve the bias in only one direction. The second sensor provides a second component that can completely solve the bias. For maximum sensitivity the second sensor should be positioned 90° from the first sensor, but as long as the sensor is not located on or near the same plane as the first sensor and the spin axis, the bias may be solved.

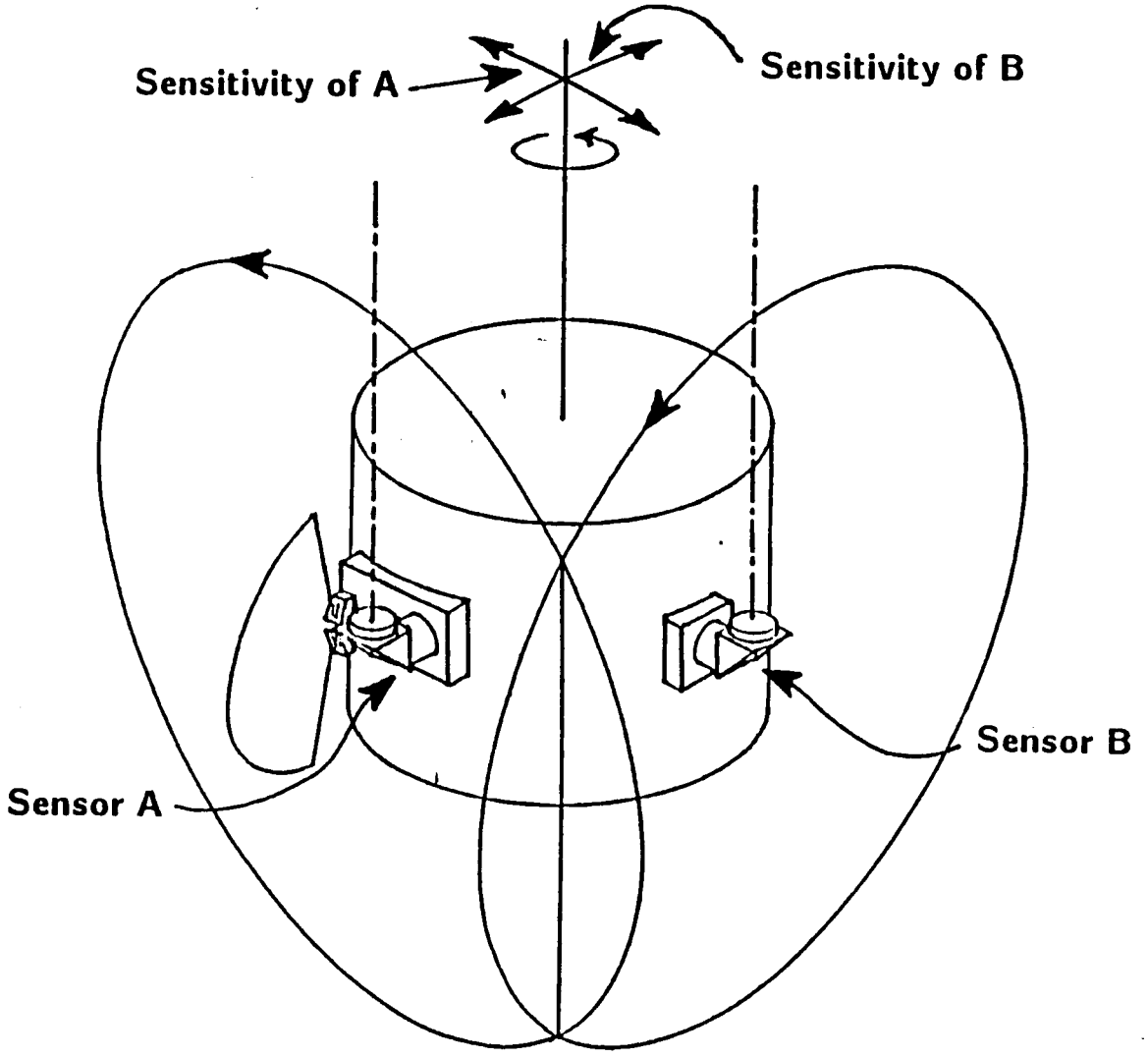

FIGURE 4.8-1
BIAS IS DIRECTLY MEASURED USING TWO SENSORS

4.9 Summary of Performance as Applied to ISTP

The following performance evaluation utilized the algorithms presented in Section 4.7.4. The inputs were single sets of synthesized scan data with resolution of 0.2°. In reality, much more data will be utilized for purposes of attitude determination. Utilizing the method of least squares, the errors will be reduced as the quantity of data is increased. Thus, the results indicated below should be considered conservative.

4.9.1 Uncertainty in Centroid Determination

The uncertainty in centroid determination depends on the apparent angular size of an object and the noise level.

Figure 4.9-1 shows a family of curves of different noise levels. With 0.05° of noise, the uncertainty in centroid determination is well below the 0.03° mark.

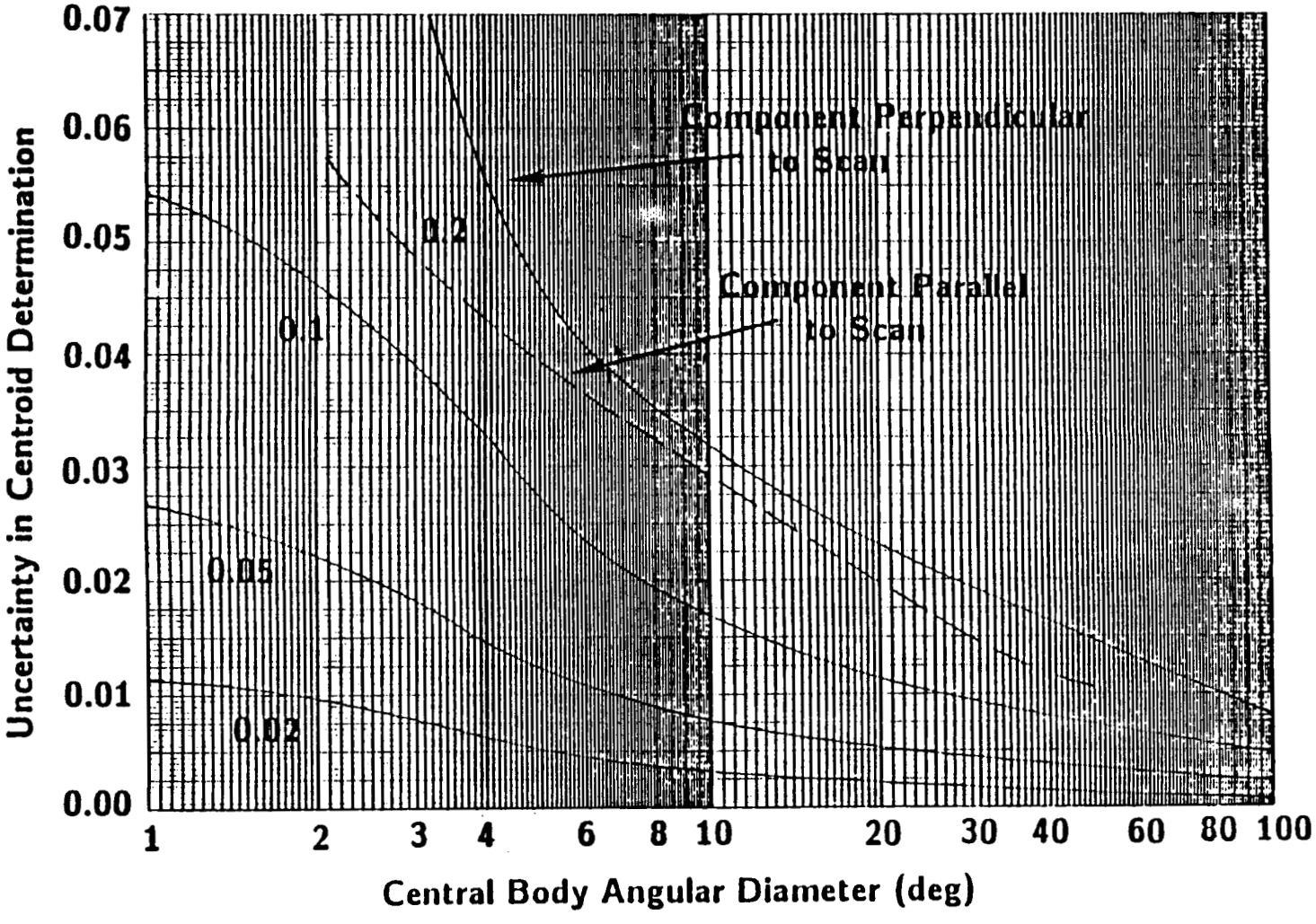

FIGURE 4.9-1
UNCERTAINTY OF CENTROID DETERMINATION

4.9.2 Attitude Determination for WIND

WIND mission presents the most challenging problem for attitude determination of all the ISTP missions. As presented in Section 4.8.3 the use of the Moon solves a singularity due to the near colinearity of the Sun, spacecraft and Earth.

Figure 4.9-2 is a graph that shows the effects of noise and the Earth-Moon elongation angle on the attitude uncertainty. Note the large improvement in attitude uncertainty as the Moon moves farther away from the Earth.

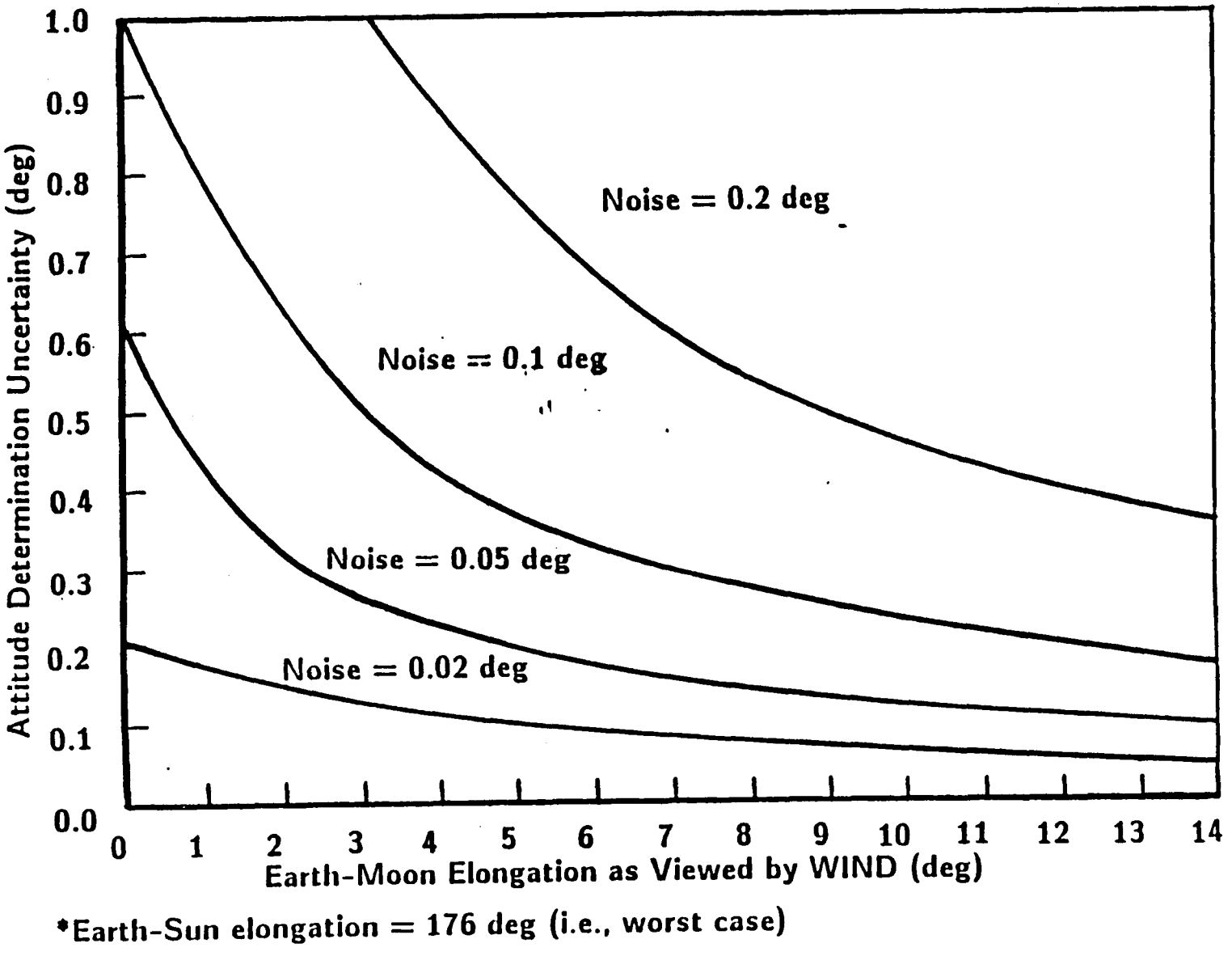

FIGURE 4.9-2
ATTITUDE DETERMINATION UNCERTAINTY
AS A FUNCTION OF NOISE AND EARTH-MOON ELONGATION

4.9.3 Summary of Attitude Determination Uncertainty

The Full-Sky Scanner will perform acceptably during the WIND, POLAR and EQUATOR Mission. Attitude uncertainty will be below 0.1° provided the Moon is available.

The worst condition for attitude determination is during the WIND Mission at L1. A singularity exists at this point that produces relatively poor results when the Moon is not used. When the Moon is utilized, the singularity is resolved and the uncertainty is improved to better than 0.1°.

Figure 4.9-3 is a graph that shows the attitude uncertainty for the WIND, POLAR and EQUATOR Missions at various positions. Uncertainty of the centroid is anticipated to be in the better than 0.03°.

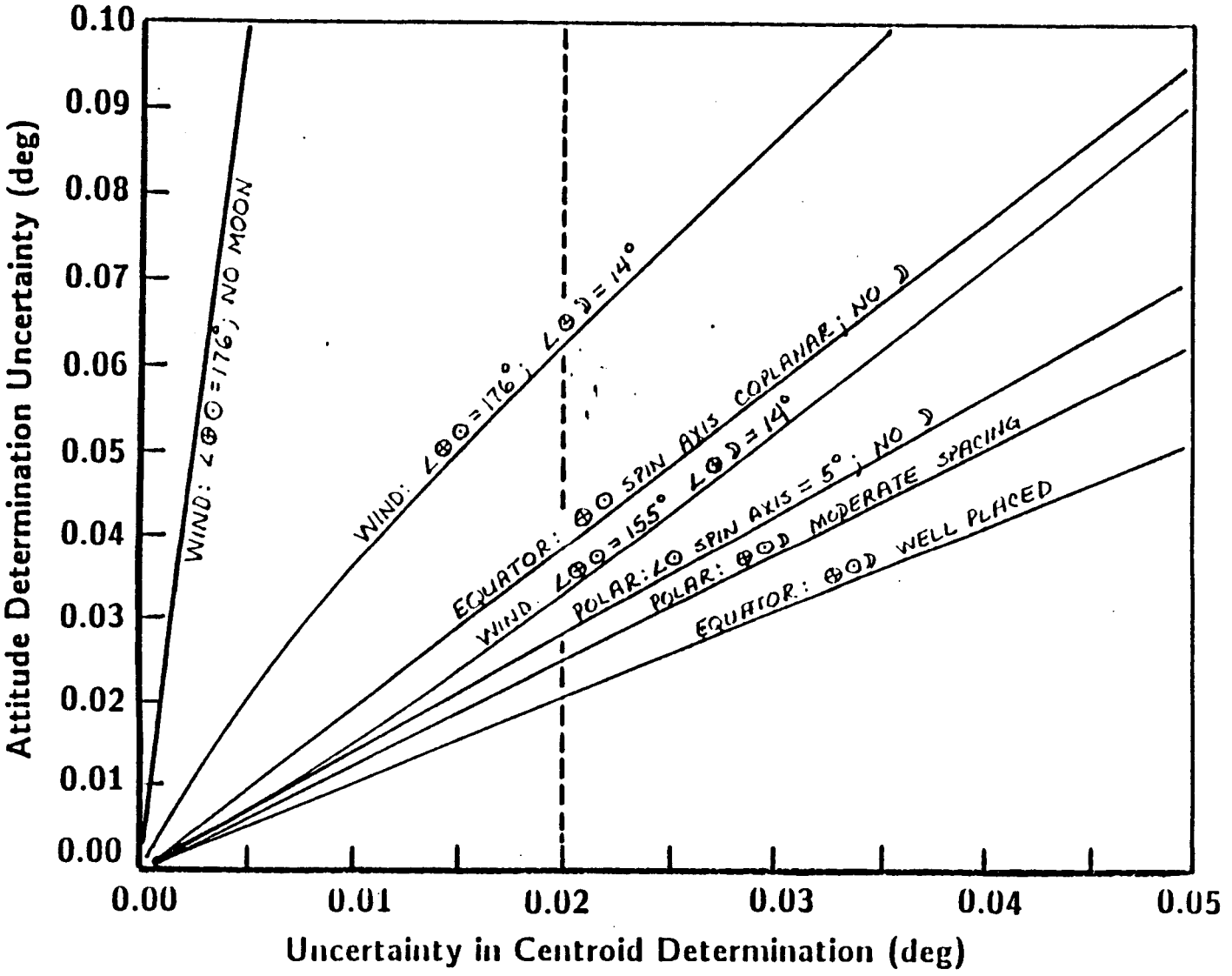

FIGURE 4.9-3
SUMMARY OF ATTITUDE DETERMINATION FOR ISTP MISSIONS

4.10 Assessment of Other Motor Options

Prior to deciding on the concept of continuously scanning the sensor, other options were investigated. These approaches increased the resolution of the stepper motor either by exotic gearing arrangements or by electrically microstepping the motor.

The mechanical approaches investigated, incorporated gearing such as the swashplate used in the Teldix stepper motor or harmonic drive used by Schaeffer. The Teldix stepper motor utilizes a swashplate to increase the resolution of a conventional stepper motor. The accuracies and resolution of this motor design approach our requirements, but there are some aspects of the design that indicate that it is not the ideal motor for our application. The life expectancy of the motor is questionable at this point and the use of a swashplate produces a coning angle between the spin axis of the motor and the housing. The coning angle will complicate the data.

The harmonic drive was another method of increasing the resolution of a stepper motor that was assessed. The approach proposed to us by Schaeffer was a considerably more complex mechanical system than our present system.

An electrical alternative to the resolution problem is microstepping. Microstepping subdivides the natural steps of the motor into smaller steps. This is done by adjusting the currents into the windings to produce an equilibrium at some intermediate step between the natural steps. The resolution of the steps is dictated by the amount of memory available to store the position to current table, the resolution of the digital to analog converter, and the bearing noise.

Microstepping offers very good resolution, but accuracy is still a problem. There are code wheels available that offer the type of resolution required, but they are expensive. The code wheel also eliminates one of the advantages of using a stepper motor; that is, it is no longer open loop.

4.11 Speed/Position Control of the Brushless DC Motor

The steady state characteristics of the speed control loop must be extremely stable. The reason for this is the small difference between the spacecraft spin rate compared to the scanning rate. For example, to produce 0.2° resolution, the scanner's spin rate must be 20.016 when the spacecraft is spinning at 20.000 RPM's. This order of control is possible with an integral control loop.

We must not only control the steady state motor speed, but also the instantaneous phase. The speed control loop must guarantee that the Earth will not be missed when scanning out 4π steradian at L1. That is, the scanner motor must not significantly deviate from its nominal track in space.

The control of the motor is only indirectly responsible for the accuracy of the acquired in-crossing and out-crossing data. The instantaneous position of the motor will be determined from the code wheel. Code wheels are available with as many as 4,096 lines (.088°). Clearly, knowledge of position is obtainable to high accuracies. Also, techniques can be used to resolve this code wheel to 0.005° (equivalent to 65,536 lines).

The resolution required in the code wheel will be a function of how well the motor can be controlled and how much controlling the motor requires. A perfectly smooth motor would only need one pulse per revolution to produce position information. The objective will be to design a motor and control loop that provides the required stability using the lowest resolution code wheel possible. The cost of the code wheel goes up rapidly as resolution is improved, so much effort will be invested in the control loop.

The viewable dimensional angle of the Moon from L1 is approximately 0.8°. That is, the one-degree FOV may be off the center of the Moon by 0.4° and still have enough signal to locate the horizon. If the scanner is in a 0.2° search mode, then worst case the nominal scan path may miss the center by 0.1°. To guarantee that the Moon is not missed, the scanner must stay within 0.3° of the nominal scan path. Thus, the brushless DC motor must track the nominal scan path to ±0.3°, and our design objective is <0.1°.

Two control schemes have been proposed. The first and most straight forward approach is to control the speed of the motor with a conventional speed control loop. Controlling the average speed of the motor over one revolution of the spacecraft is relatively easy. The trick will be to get the bandwidth of the control loop up high enough to be able to control the phase of the motor against the bearing noise.

The brushless DC motor will be designed in Phase II. For purposes of this report, assume the brushless DC motor has the following characteristics:

Resistance of Windings (R): 40 Ω
Inductance of Windings (L): 30 mH
Coefficient of Viscous Friction (B): 0.3939 oz-in/(rad/sec)
Moment of Inertia (J): 62×10^{-3} oz-in - s^2
Torque Constant (K_T): 55 oz-in/amp
Back EMF: 1 V/(rad/sec)

NOTE: These characteristics are from an existing ITHACO motor used in the Conical Earth Sensor.

Figure 4.11-1 is a block diagram of the brushless DC motor. The transfer function of the motor is then:

$$\frac{\theta}{V_{in}} = \frac{29{,}569}{S^2+1{,}339.7S+38{,}041} = \frac{29{,}569}{(S+1{,}311)(S+29)} \text{ or } \frac{.777}{(1+763\times10^{-6}S)(1+34.5\times10^{-3}S)}$$

The worst offender to speed stability will be the bearing noise. To get an idea how the noise will effect the motor, two simulations were performed on the computer.

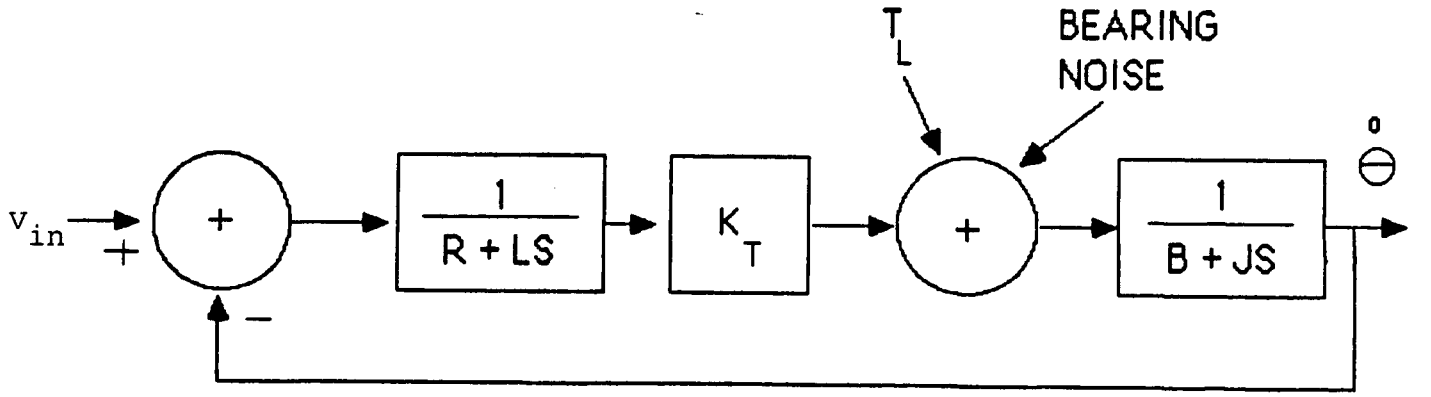

FIGURE 4.11-1
MODEL OF BRUSHLESS DC MOTOR

The first simulation indicated how an open loop motor would respond to the bearing noise. Figure 4.11-2 is a graph of the results. The top trace is the speed of the motor. The center trace is the bearing noise that was injected into the model. The third (bottom) trace is the position (phase) error. The position error was divided by subtracting the steady state speed of the motor (without noise injected) from the motor's speed, then integrating. It is clear that the position error is outside the allowable limit of ±0.1°, and that a tack loop must be used to provide faster response in the motor controller.

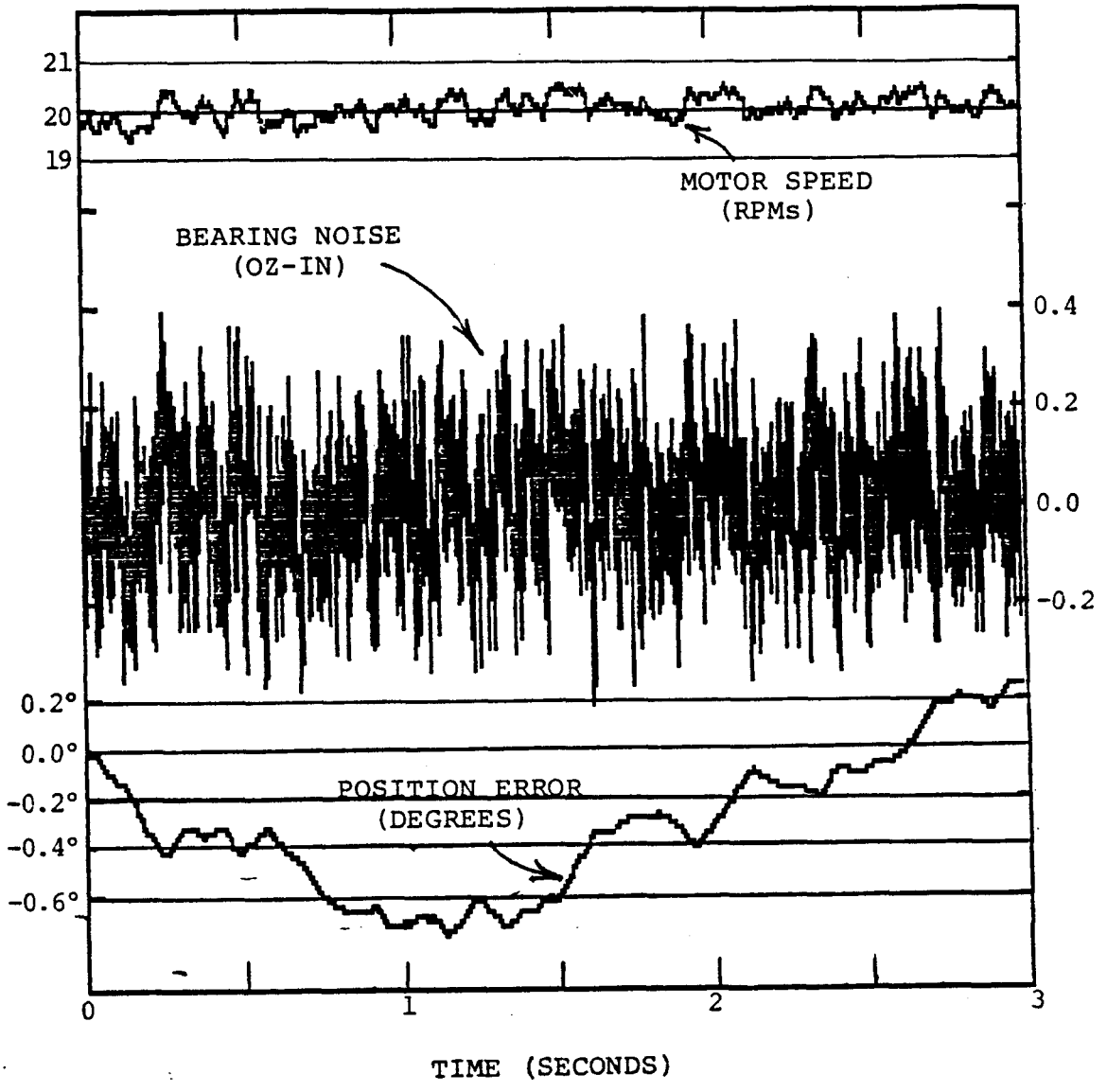

FIGURE 4.11-2
COMPUTER SIMULATION OPEN-LOOP BRUSHLESS DC MOTOR

The following shows the improvement achieved by a simple speed controller.

A speed control loop is shown in Figure 4.11-3. A one-shot is fired by every 1/2 cycle on the code wheel, then the signal is filtered to produce the feedback. To simulate position firing of the one-shot on the computer, the speed is integrated then a signal is produced every 1/8°. This simulates a code wheel with marks every 1/4°. The one-shot produces a signal with an amplitude of one, the pulse width is 500 microseconds. The filter that follows has a time constant of 1 millisecond.

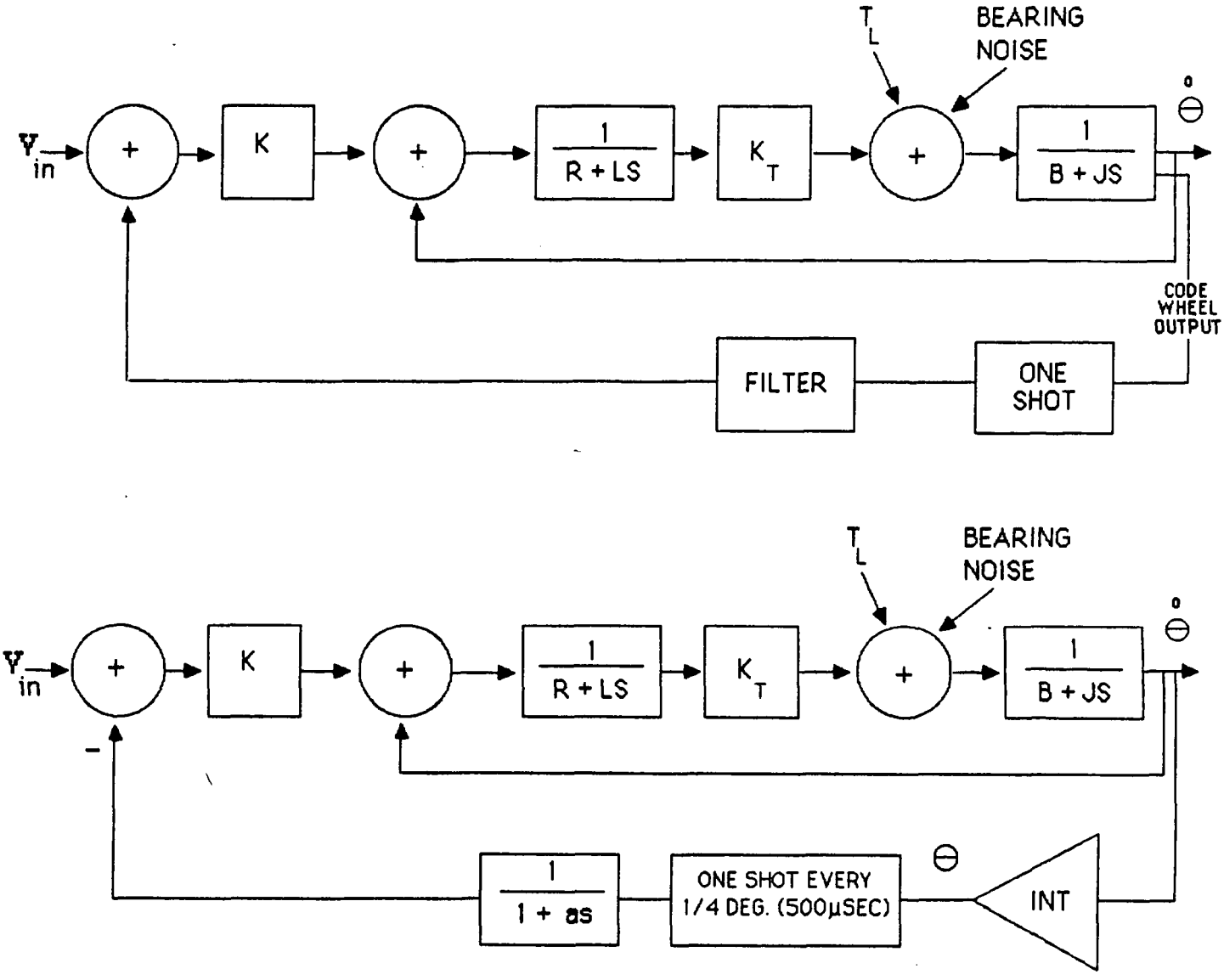

FIGURE 4.11-3
SPEED CONTROL LOOP

a) Basic Control Loop
b) Control Loop Implementation on the Computer

Figure 4.11-4 shows the improved performance of the motor with the speed control loop. This control loop adequately holds the motor to about 0.1° with respect to the nominal position path.

An alternative to controlling speed is to control the position by phase locking the motor with the spacecraft. This approach appears to be sound, but it is more complicated than the speed control approach. Interconnecting phase lock loops presents a complicated analysis problem. This approach is available but should be used only in the event that the speed control scheme does not pan out.

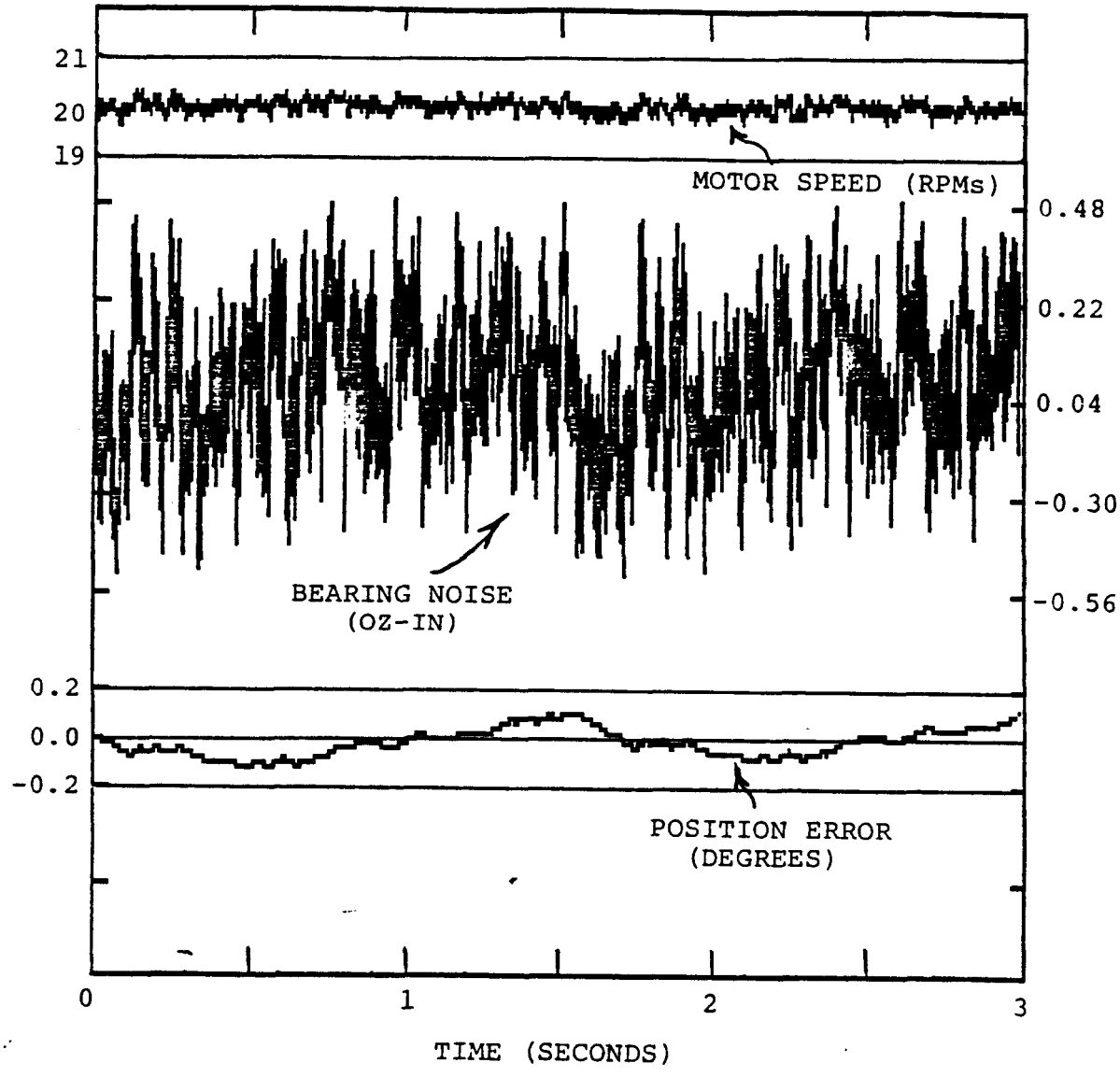

FIGURE 4.11-4
COMPUTER SIMULATION SPEED CONTROL LOOP

4.12 Pyroelectric Detector Investigation

Pyroelectric detectors are commonly used in horizon crossing indicators, and have three significant advantages over the thermister bolometer:

1. The sensitivity is higher, giving better signal to noise ratio. This is desirable for more reliable detection of the Earth and Moon at long distances.

2. No biasing of the detector is required, thus simplifying the circuitry, and minimizing 1/f noise.

3. The device geometry for a given field of view is much larger. This makes it easier for precision alignment of the detector within the sensor.

For these reasons, laboratory investigations of pyroelectric detectors were undertaken.

4.12.1 Discussion of Experiments

4.12.1.1 Devices Tested

Two different pyroelectric detectors were available for experimentation. One was a plain detector manufactured by Laser Precision Corporation (P/N J-506-P5). The second detector was manufactured by Infrared Associates Incorporated. It has a FET built in to amplify the detector signal. The plain detector was very difficult to use. Pickup, microphonics, signal droop etc., made quantification very difficult. We got some signal out, but were not impressed.

The device with the built in FET was another matter. We installed that device in an HCI barrel. The internal FET was used as a source follower to buffer the detector output. Results on the optical bench and the Earth simulator were encouraging. Microphonics were minimal and signal amplitude was good. All of the following data and analysis is based upon this device.

4.12.1.2 Earth Simulator Experiments

The pyroelectric detector was installed in an HCI with 14 to 16 micron optics. The HCI was first checked out on the optical bench with a chopped source. The pyroelectric detector gave a good signal with slow rise and fall time. We also checked it against a 230 Kelvin equivalent Earth target. Signal droop was satisfactorily low. The output resembled a bolometer output signal to a surprising degree. We then added a lead amplifier to the electronics to cancel out the residual pole such as is currently done in the CES to cancel the bolometer's thermal lag. Typcial transfer functions are given in Section 4.12.1.3.

4.12.1.3 Transfer Functions of Bolometer Pyroelectric Detector Circuits

Typical transfer functions of the electronics, including compensations for the thermal lag in the detectors are:

Bolometer

$$\frac{(1 + .002\ S)\ (1 + 0.3 \times 10^{-6} S)}{(1 + 3.3 \times 10^{-6} S)\ (1 + 38.3 \times 10^{-6} S)\ (1 + 823.2 \times 10^{-6} S)}$$

Pyroelectric

$$\frac{(1 + .039\ S)\ (1 + 0.3 \times 10^{-6} S)}{(1 + 3.3 \times 10^{-6} S)\ (1 + 38.3 \times 10^{-6} S)\ (1 + 823.2 \times 10^{-6} S)}$$

Under these conditions, the pyroelectric detector's signal-to-noise ratio is as good or better than that of the bolometer.

4.12.2 Effects of Peaking

4.12.2.1 Measured Signals

The following waveform photograph was taken on the optical bench with the peaking set on the basis of compensating the thermal lag. This is approximately where we would expect to set it in practice. The top trace is the amplified pyroelectric detector signal. The bottom trace is the peaked signal. Peaking has effectively removed the thermal lag of the detector and provided a square wave with overshoot. The pulse width is about 50 milliseconds.

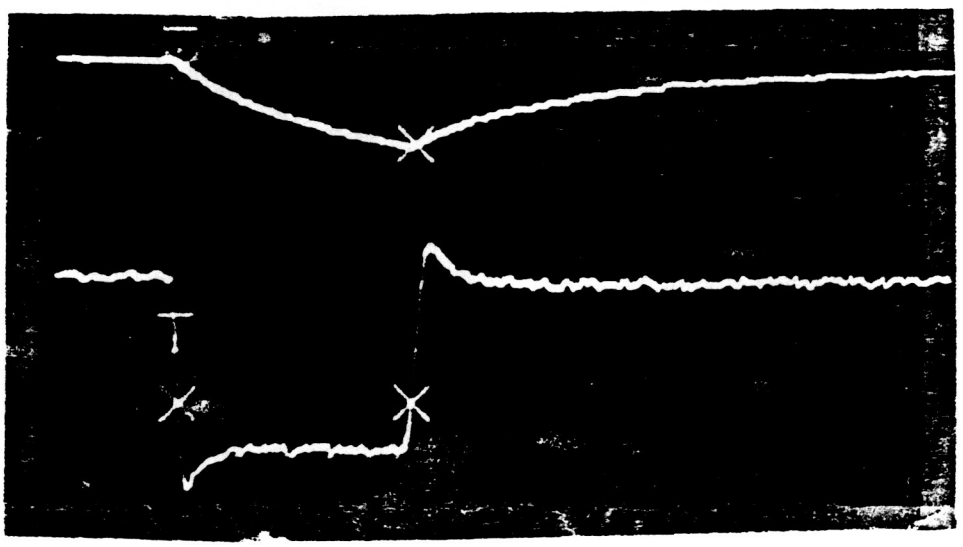

To those readers familiar with such waveforms, the peaked waveform appears to be over peaked as evidenced by the overshoot at the start and the end of the pulse. Such is not the case since there was no electronic peaking in the circuit at frequencies which could cause the overshoot. We were carefully bucking out only the thermal lag of the device. The electronics were examined by injecting a simulated pyroelectric detector signal and confirmed that the over-peaking was not in the electronics. If the peaking is real and is inherent in the pyroelectric detector, then it implies that one of the "cosmetic" poles in the transfer function could be moved down in frequency to compensate, thus significantly reducing the noise bandwidth without detracting from the signal. It has been estimated that further noise reductions up to several times might prove to be possible. More work will be done in Phase II.

5.0 SUMMARY

A modification of an existing sensor has been analyzed for a Full-Sky Scanner for a spinning or dual spin spacecraft. The scanner can locate the Sun, Earth and Moon anywhere between low-Earth orbit to 250 Earth radii away. Attitude may be determined with an uncertainty of less than 0.05 degrees in most cases. The modifications are minor and the risk is low.

5.1 General Overview

The Full-Sky Scanner utilizes a brushless DC motor to spin the scanner. With the scanner rotating othogonally to the spin axis of the spacecraft, and the speed of the scanner properly controlled, the scan pattern can be moved across the sky. Resolution between scan paths is strictly a function of the relative speeds between the motor and the spacecraft.

It was shown that the worst case signal levels occur at L1. Here the Moon is detectable over a viewable angular distance of 0.8° while the Earth is 1.0°. A fixed radiance locator was shown to provide optimum performance. This analysis was based on conservative assumptions; therefore, better detection is expected.

A pyroelectric detector was investigated and found to have advantages over the bolometer. If this device were incorporated there would be an improvement in detectability.

Effects of bearing noise and speed control loops were evaluated. The instantaneous position can be held to 0.1° of the nominal position.

An algorithm for determining the attitude of a spacecraft was presented. The algorithm first determines the centroid of an object given in-crossing and out-crossing telemetry data. Secondly, the algorithm solves for the attitude using the ephemeris.

5.2 System Performance

Accuracy of better than 0.05° (3σ) is expected for nearly all conditions. The most severe attitude determination problem occur at L1 during the mission. The Moon must be utilized to resolve a singularity. Attitude accuracy will be better than 0.1° even at L1.

Attitude determination at low Earth orbit may be compromized by opening the passband filter to produce better results at higher earth orbits. Worst case errors of Earth detection based on a single scan at low orbits will be less than 0.5°.

6.0 PHASE II TASKS

The primary effort in Phase II will be to design and build a Breadboard Full-Sky Scanner. The Breadboard will be manufactured using high quality non screened flight grade hardware. Informal environmental testing will be conducted to evaluate performance over temperature in a vacuum, etc. The following tasks are required to meet this end.

- Design a Brushless DC Motor for the Existing Sensor
  - Code wheel selection
  - Speed control loop
- Select an Infrared Detector
  - Further investigation work required to assess temperature and radiation effect on pyroelectric detectors.
  - Further assessment of the thermal response of the pyroelectric detector is required.
- Design Associated Electronics
  - Locator for Sun
  - Locator for Earth and Moon
  - Telemetry interface electronics
  - Control electronics
- Bias Determination - Including Identification of All Bias Terms and How to Treat Them
  - Constant cone-angle bias
  - Mounting angle biases
  - Inter-sensor biases
- Design and Build Required Test Equipment
- Operator Modes - Define and Incorporate
  - Search mode
  - Dither mode
  - Assessment of full-sky scan time

ATTACHMENT

SHCI SALES BROCHURE

- The SCHI is being successfully used on the USAF P78–2 (SCATHA) Spacecraft that was launched on January 30, 1979.

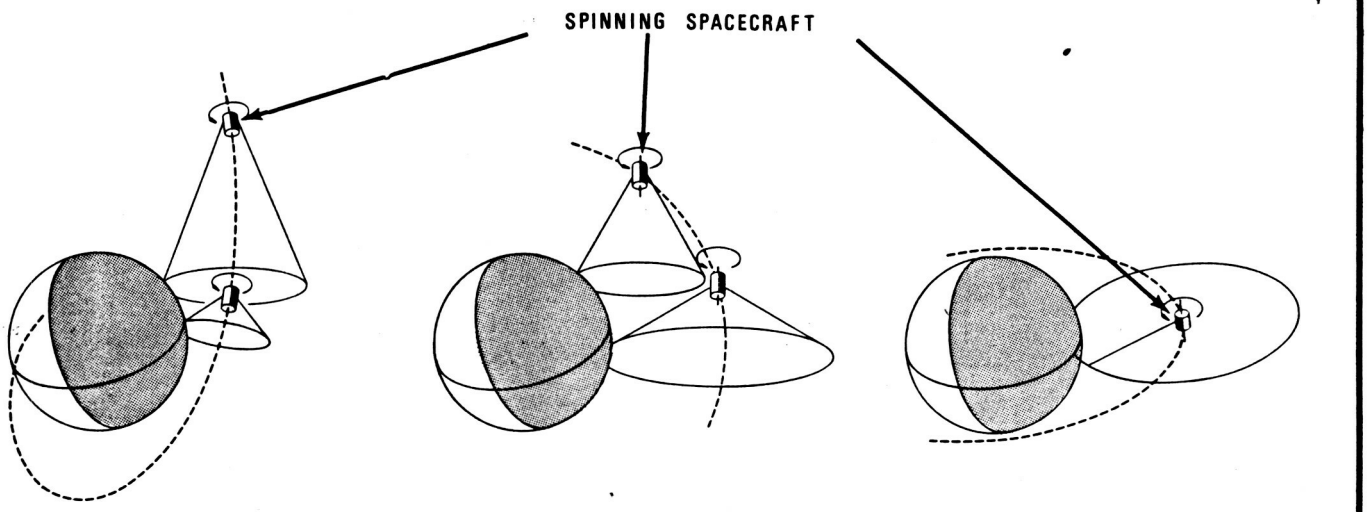

Possible SHCI Applications

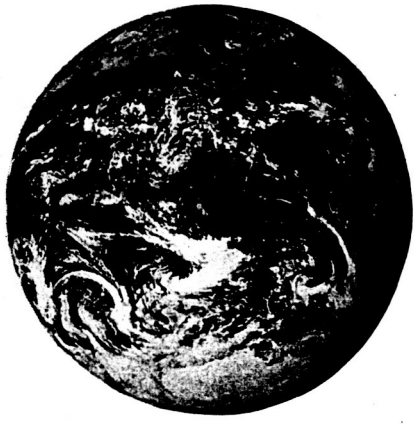

For more information on this and other ITHACO Space Products
contact M. Z. Rutkowski, Division Manager, Spacecraft Instruments Division

ITHACO, INC 735 WEST CLINTON STREET BOX 6437 ITHACA, NEW YORK 14851 USA
PHONE 1–800–847–2080 or 607–272–7640 TWX 510–255–9307

PRINTED IN USA

Specifications

APPLICATION	For spinning space vehicle launch phase, transfer orbit, on–orbit (elliptical or circular, any inclination)
SPACECRAFT SPIN RATE	1 to 200 rpm
INSTANTANEOUS FIELD OF VIEW	$1° \times 1°$
FIELD OF VIEW COVERAGE	$0° - 360°$
INCREMENT (120 steps) @	3°
STEP RATE	0 to 200–steps/sec
OPTICAL PASSBAND	$14 - 16\mu$
ACCURACY	$0.1°$ (3σ)
ALTITUDE RANGE	150 – 60000 km
SIZE Sensor – Electronics–	13.34 x 9.14 cm (max dia) 15.24 x 15.24 x 5.23 cm
WEIGHT	1.6 kg
POWER	2.5W static +7.5W when stepped

A 45 degree fold mirror is mounted to a ball–bearing suspended housing driven by a stepper motor. A position sensor in conjunction with an up–down counter provides the line of sight position information for all incremental position settings. The SHCI's signal outputs (line of sight position and the horizon location) are used for attitude determination of the spacecraft.

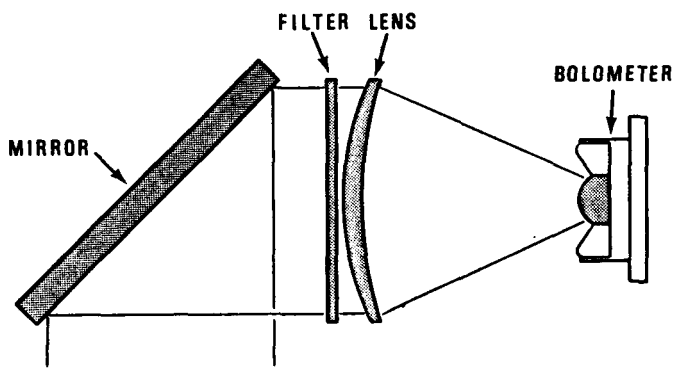

ISS Optical Diagram

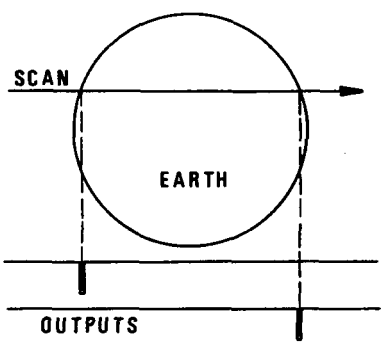

SHCI Scan Pattern and Signal Output

SHCI

Steerable Horizon Crossing Indicator

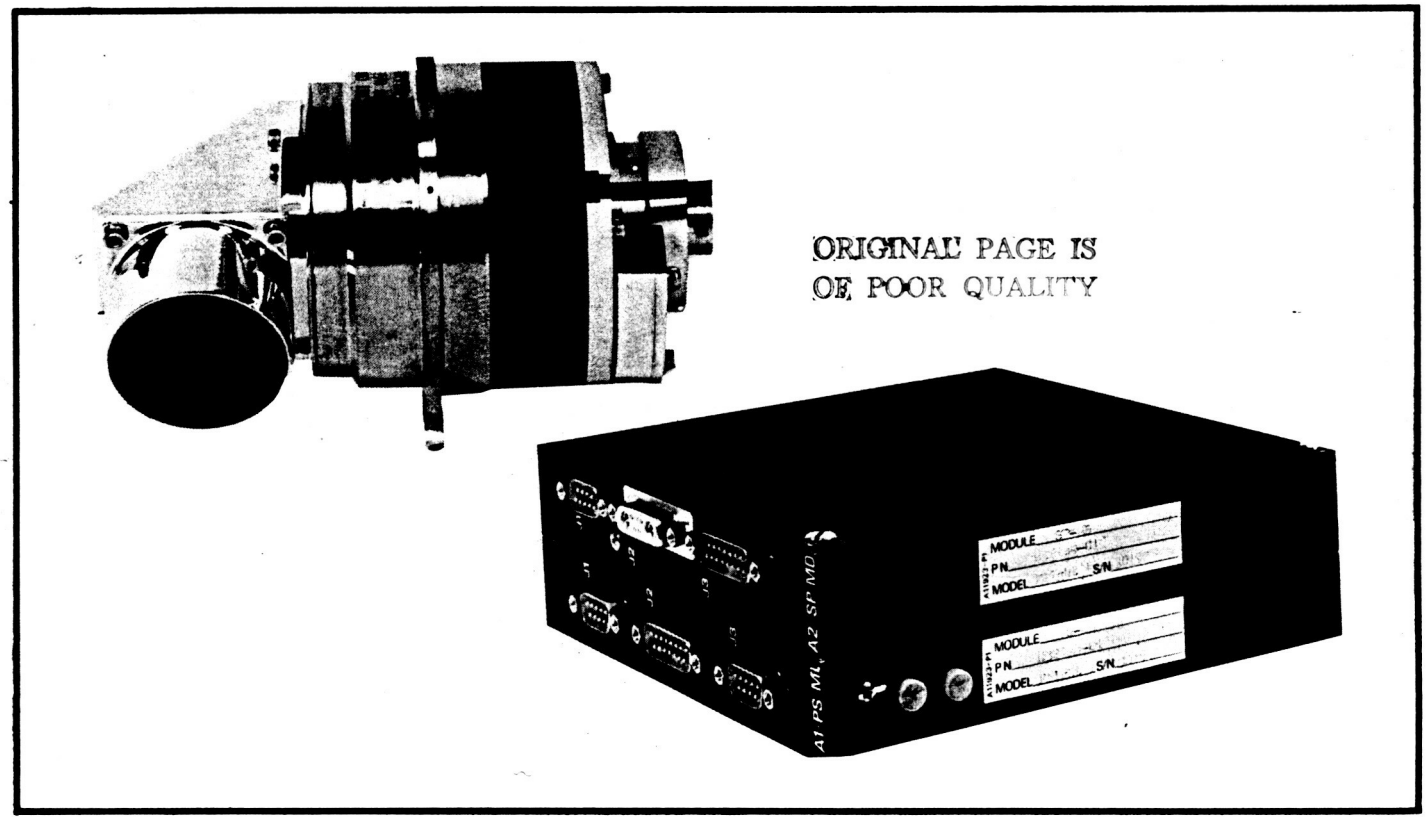

Description

The Steerable Horizon Crossing Indicator (SHCI) is intended for use on a spinning Space Vehicle. It senses the thermal discontinuity between Earth and Space as the line of sight crosses the horizon. The SHCI's line of sight is adjustable in 3° increments by command over the full 360°.

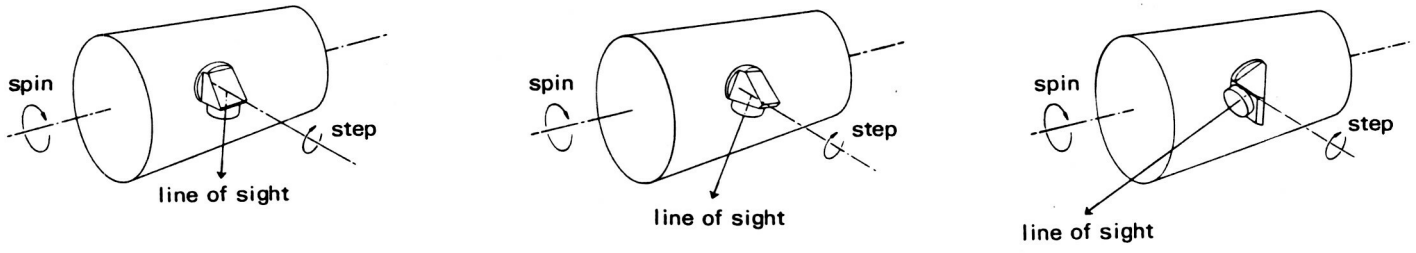

Spacecraft Mounting Configuration

ITHACO

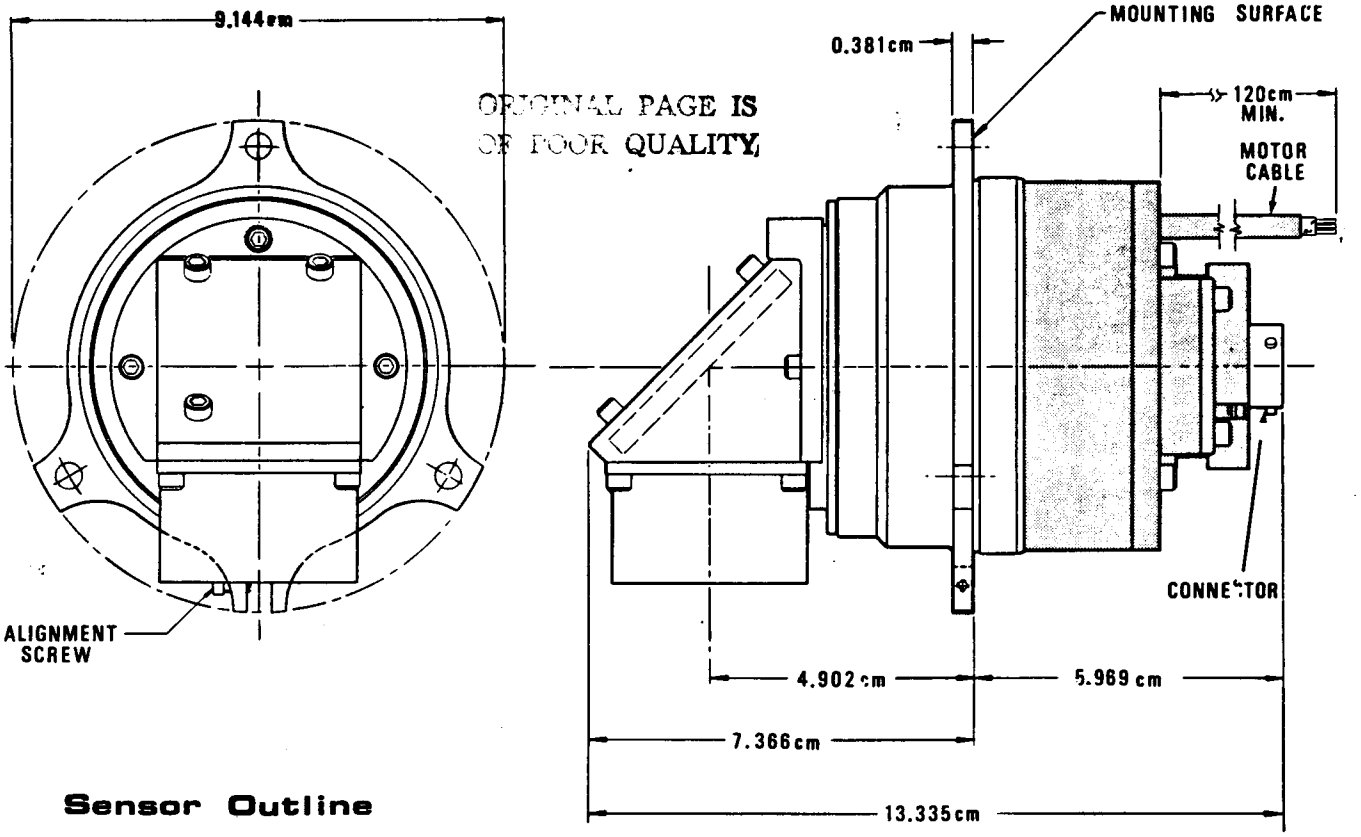

Sensor Outline

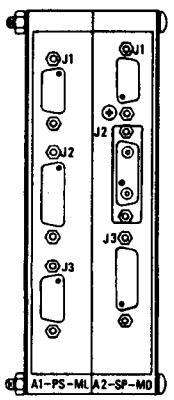

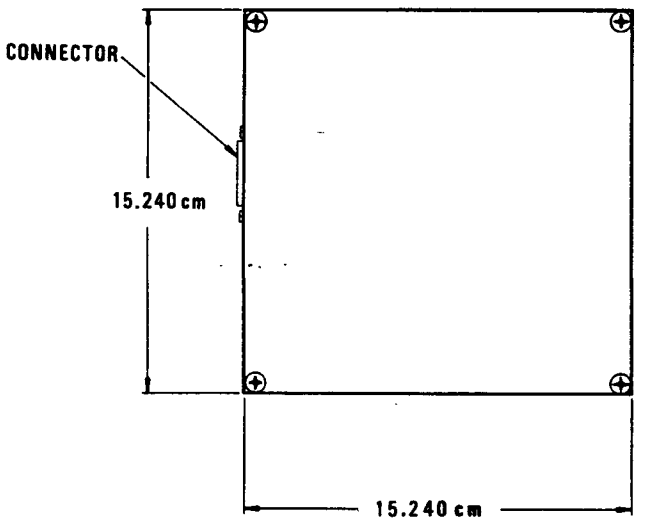

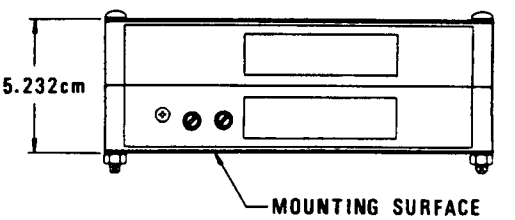

Electronics Outline